

Postersession
Wednesday 11.03.2020
15:00 – 16:30

Influence of the surface morphology on the defect distribution in the faceted region of 4H-SiC single crystals

Matthias Arzig^a, Michael Salamon^b, Ta Ching Hsiao^c, Norman Uhlmann^b and Peter J. Wellmann^a

^a Crystal Growth Lab, Materials Science Department 6, Friedrich-Alexander-Universität Erlangen-Nürnberg, Martensstraße 7, 91058 Erlangen, GERMANY

^b Fraunhofer Institute for Integrated Circuits, Development Center for X-Ray Technology (EZRT), Flugplatzstraße 75, 90768 Fürth, Germany

^c Industrial Technology Research Institute of Taiwan (ITRI), 195, Sec 4, Chung Hsing Rd., Chutung, Hsinchu 31040, Taiwan (TaChingHsiao@itri.org.tw)

For the growth of silicon carbide (SiC) crystals, the physical vapor transport (PVT) method has matured to become the industrial standard route [1-4]. The wafer quality has improved continuously making micropipe (MP) free material commercially available. By the optimization of the process conditions, the generation of new defects during growth is reduced as far as possible, leading to a steady reduction of defect densities in the wafers. Besides the suppression of defect formation also a distinct reduction of defects is possible in SiC crystals, for example by the conversion of defects as observed in the solution growth method [5]. It is believed that due to high surface steps threading defects are deflected into the basal plane. Using our in-situ computed tomography system we can observe the effect of changed process conditions directly during the growth. A different evolution of the growth interface shape was observed during crystal growth runs, caused by the application of insulation materials of differing thermal conductivity. A higher thermal conductivity leads to a larger radial thermal gradient in front of the growing crystal as confirmed by numerical simulation. Insulation material with lower thermal conductivity leads to a smaller radial temperature gradient at the crystal growth interface. Therefore, differently shaped growth interfaces evolve and different step morphologies are formed.

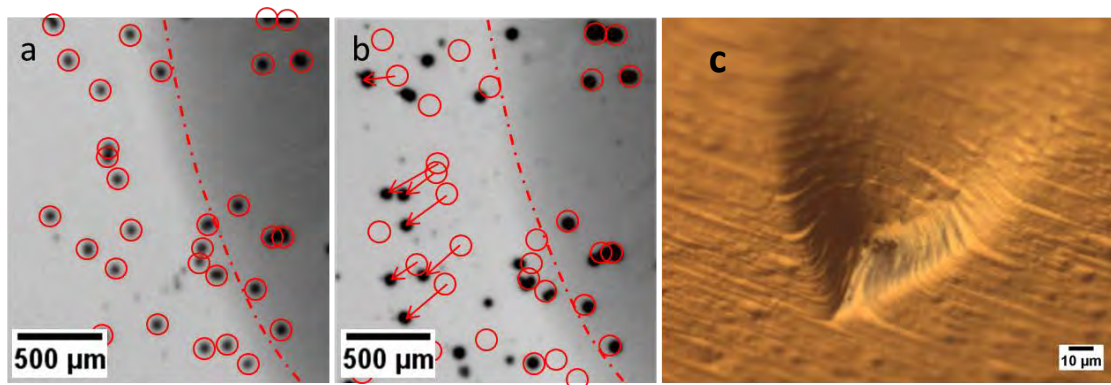


Fig. 1: micropipes in the stepflow area changing their position from bottom (a) to top (b) in the crystal.
(c) micropipe penetrating the crystal surface in the step-flow area

Due to the higher radial temperature gradient a smaller facet and steeper crystal flanks evolved compared to the growth run using an insulation material of lower thermal conductivity. The steep crystal flanks feature high surface steps as visible in Figure 1c, which strongly interact with the crystal defects. Two different mechanisms for the bending of micropipes (MPs) away from the $[1\bar{1}00]$ direction were found. Figure 1 a and b depicts the step flow area where the MPs are deflected collectively in the direction of the step flow by big surface steps. In the facet area the repulsive interaction of selected MPs led to a slight deflection restricted to the $\{1\bar{1}00\}$ prismatic plane in the $\langle 11\bar{2}0 \rangle$ direction as depicted in Figure 2, caused by repulsive interaction.

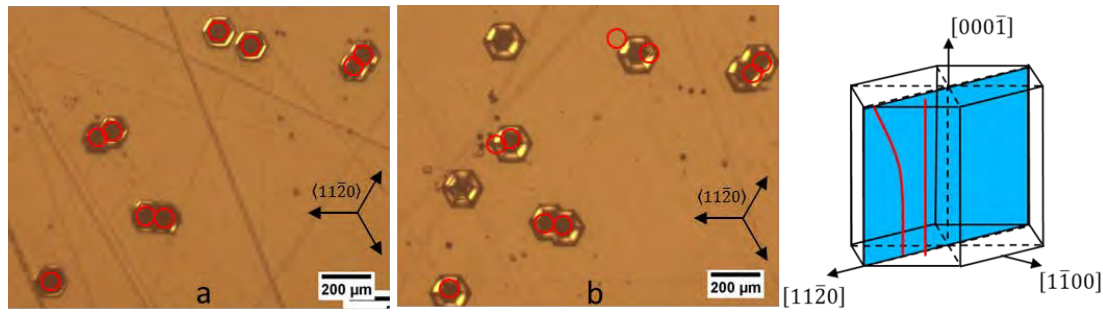


Fig. 2: micropipes in the facet area changing their position from bottom (a) to top (b) in the crystal.
(c) illustration of the repulsive interaction of two MPs with the same burgers vector

The defect densities listed in table 1 indicate that the large surface steps on the surface of crystal B convert a large amount of TEDs into BPDs leading to a reduction of this defect during the growth process.

Table 1: Densities of defects for crystal A grown under smaller radial thermal gradient and Crystal B grown under larger radial thermal gradient. Wafer #1 denotes the Wafer closer to the growth surface and Wafer #2 denotes the Wafer closer to the seed, respectively.

	TED [$1/\text{cm}^2$]	TSD [$1/\text{cm}^2$]	BPD [$1/\text{cm}^2$]
Crystal A Wafer #1	$(2.33 \pm 0.03)\text{E}4$	$(0.94 \pm 0.02)\text{E}3$	$(4.58 \pm 0.05)\text{E}3$
Crystal A Wafer #2	$(2.18 \pm 0.02)\text{E}4$	$(1.00 \pm 0.03)\text{E}3$	$(5.27 \pm 0.05)\text{E}3$
Crystal B Wafer #1	$(0.44 \pm 0.08)\text{E}4$	$(0.88 \pm 0.29)\text{E}3$	$(3.14 \pm 0.61)\text{E}3$
Crystal B Wafer #2	$(1.12 \pm 0.30)\text{E}4$	$(1.00 \pm 0.33)\text{E}3$	$(3.07 \pm 0.58)\text{E}3$

For the growth of large SiC boules the application of large radial gradients for defect reduction seems not appropriate as large radial strain will lead to the generation of new defects. Therefore, the application of an off-axis angle to produce a surface morphology featuring large steps would be a better method. Measurements of the angle between the facet plane and the crystal flanks, reveal an inclination angle of 10° directly around the rim of the facet and going up to 20° further away at the steepest regions. The growth on seeds cut with a large off-axis angle between $10\text{-}20^\circ$ can be a promising approach to achieve defect reduction in PVT grown SiC by large surface steps, while avoiding large radial thermal gradients.

Acknowledgment

The authors acknowledge funding by the DFG under the grant numbers WE2107/12-1 and UH246/4-1

- [1] I. Manning, G. Y. Chung, E. Sanchez, Y. Yang, J. Q. Guo, O. Goue, B. Raghathamachar, M. Dudley, Materials Science Forum, **924**, 11-14 (2018)
- [2] A. R. Powell, J. J. Sumakeris, Y. Khlebnikov, M. J. Paisley, R. T. Leonard, E. Deyneka, S. Gangwal, J. Ambati, V. Tsevtkov, J. Seaman, A. McClure, C. Horton, O. Kramarenko, V. Sakhalkar, M. O'Loughlin, A. A. Burk, J. Q. Guo, M. Dudley, E. Balkas, Materials Science Forum, **858**, 5-10 (2016)
- [3] T. L. Straubinger, E. Schmitt, S. Storm, M. Vogel, A. D. Weber, A. Wohlfart, Materials Science Forum, **645-648**, 3-8 (2010)
- [4] A. K. Gupta, P. Wu, V. Rengarajan, X. P. Xu, M. Yoganathan, C. Martin, E. Emorhokpor, A. Souzis, I. Zwieback, T. Anderson, Materials Science Forum, **717-720**, 3-8 (2012)
- [5] S. Harada, Y. Yamamoto, S. Xiao, D. Koike, T. Mutoh, K. Murayama, K. Aoyagi, T. Sakai, M. Tagawa, T. Ujihara, Materials Science Forum, **821-823**, 3-8 (2015)

Limitations during Vapor Phase Growth of Bulk (100) 3C-SiC Using 3C-SiC-on-SiC Seeding Stacks

M. Schöler^a, P. Schuh^a, J. Steiner^a, F. La Via^b, Marco Mauceri^c, Marcin Zielinski^d,
Peter J. Wellmann^a

^a Crystal Growth Lab, Materials Department 6 (i-meet), FAU Erlangen-Nuremberg, Martensstr. 7,
D-91058 Erlangen, Germany

^b CNR-IMM, sezione di Catania, Stradale Primosole 50, I-95121 Catania, Italy

^c LPE S.P.A., Sedicesima Strada, I-95121 Catania, Italy

^d NOVASiC, Savoie Technolac, BP267, F-73375 Le Bourget-du-Lac Cedex, France
E-mail: michael.schoeler@fau.de

Summary

Certain condition including a high supersaturation, a silicon-rich gas phase and a high vertical temperature gradient during the growth of 3C-SiC are key challenges to obtain high quality material. We have developed a transfer method creating high-quality 3C-SiC-on-SiC (100) seeding stacks, suitable for use in the so-called sublimation “sandwich” epitaxy (SE) [1]. A series of growth runs with different source to seed distances were performed and characterized by XRD and Raman spectroscopy. The measurements revealed a decrease in material quality with increasing source to seed distances.

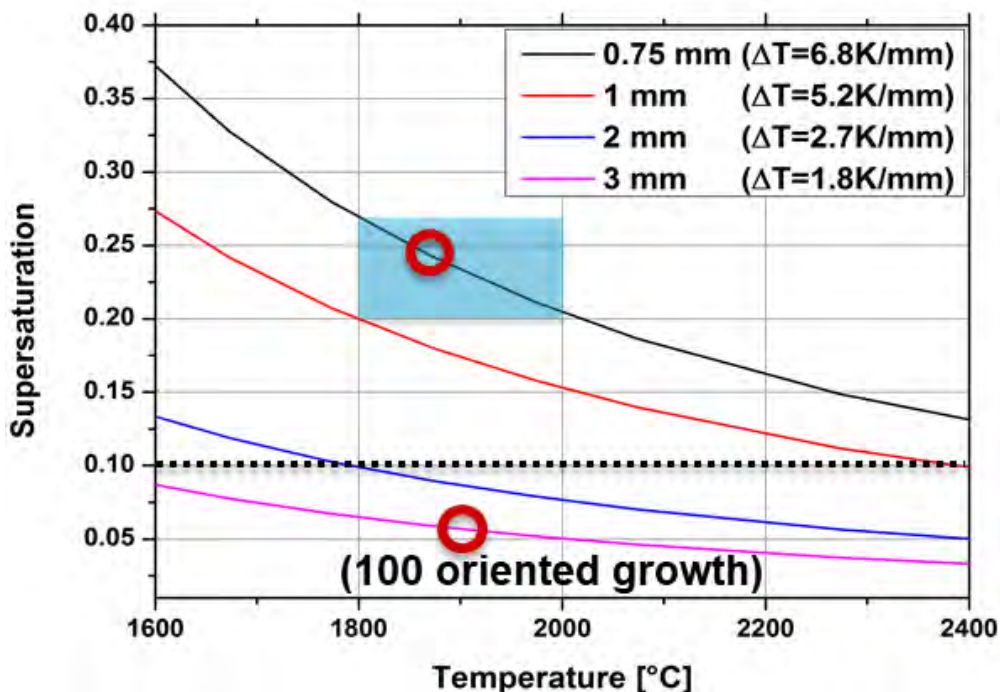


Fig. 1: From simulation data calculated supersaturation of the growth-limiting gas species SiC₂ as a function of temperature for varying source-to-substrate distances. Highlighted areas are extracted from the literature and experiments were performed on (100)-oriented material. The dashed line marks the minimal necessary supersaturation for stable growth of 3C-SiC.

For a better understanding, simulations of the used SE setup were carried out using COMSOL Multiphysics. Thereby a quantitative estimation for the temperature gradient and consequently the supersaturation of the growth limiting gas species SiC_2 was created. Different source-to-seed distances were taken into account as well as various temperatures. The simulated data showed a decrease in supersaturation of the growth-limiting SiC_2 gas species with increasing source-to-seed distances (Fig. 1). The observed decline in crystal quality during the growth runs with increasing spacing could therefore be explained by the reduction in supersaturation.

The main defect limiting the growth of cubic silicon carbide appears to be the protrusion defect which is already present in the seeding layers [2]. Morphology analysis of as-grown material indicates an increasing protrusion dimension with increasing crystal thickness. This effect limits the achievable maximal thickness. During growth of an approximately 2.7 mm thick crystal additional polytype inclusions could be observed. They began to occur at low supersaturation ($S \leq 0.06$) and prolonged during growth (increase of carbon gas-species). Nevertheless, switch-backs to the cubic polytype could be observed at later growth stages. Together with the simulated data, we were therefore able to suggest a necessary minimal supersaturation of 0.1 for the stable growth of 3C-SiC.

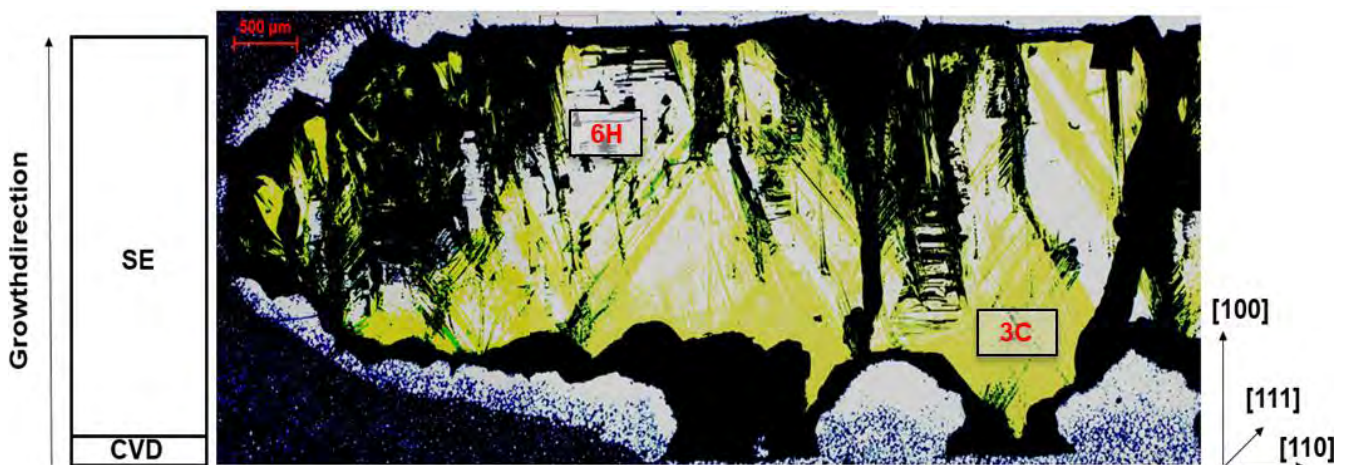


Fig. 2: Crosscut from an approx. 2.7 mm thick one-inch sample in through-light set up viewed with an optical microscope. The growth conditions were near the limit of stable 3C-SiC growth (yellow areas) as can be seen by the white inclusions representing polytype switches to 6H. Backside sublimation also occurred during the growth (removed areas located at the bottom).

Acknowledgment

This work is funded by the European H2020 framework program for research and innovation under grant agreement number 720827 (CHALLENGE).

[1] P. Schuh, M. Schöler, M. Wilhelm, M. Syväjärvi, G. Litrico, F. La Via, M. Mauceri, P.J. Wellmann, Sublimation growth of bulk 3C-SiC using 3C-SiC-on-Si (100) seeding layers, *J. Cryst. Growth*, **478**, 159-162 (2017).

[2] F. La Via, A. Severino, R. Anzalone, C. Bongiorno, G. Litrico, M. Mauceri, M. Schoeler, P. Schuh, P.J. Wellmann, From thin film to bulk 3C-SiC growth: Understanding the mechanism of defects reduction, *Mater. Sci. Semicond. Process*, **78**, 57–68 (2018).

X-Ray Analysis of Defects in 4H-SiC

M. Roder^a, J. Steiner^b, B. Nguyen^c, S. Haaga^{a,d}, M. Kabukcuoglu^{a,d}, S. Bode^d, D. Hänschke^d,
T. Baumbach^{d,e}, P. Wellmann^b, S. Sandfeld^c, A. Danilewsky^a

^a Crystallography, Albert Ludwigs University Freiburg, 79104 Germany

^b Crystal Growth Lab, Material Department 6 (i-meet), University of Erlangen-Nürnberg, 91058 Erlangen

^c Micromechanical Materials Modelling (MMM), Institute of Mechanics and Fluid Dynamics, Technical University Bergakademie Freiberg (TUBAF), Lampadiusstr. 4, D-09599 Freiberg

^d Laboratory for Applications of Synchrotron Radiation (LAS), Karlsruhe Institute of Technology (KIT), D-76131 Karlsruhe, Germany

^e Institute for Photon Science and Synchrotron Radiation (IPS), Karlsruhe Institute of Technology (KIT), D-76344 Eggenstein, Germany

E-mail: melissa.roder@krist.uni-freiburg.de

Silicon carbide (SiC) used as semiconductor material for high power devices often degrades the device's performance by a high variety and density of defects [1]. The wafers of several 4H-SiC crystals, grown by Physical Vapor Transport [2, 3] at various growth conditions were characterized. For each crystal, one wafer close to the crystal seed and one wafer close to the crystal cap was investigated. Synchrotron White Beam X-ray Topography (SWXRT) measurements in back-reflection geometry were carried out at the topography station at imaging cluster of KIT light source [4] to investigate and distinguish the different defect types. Further, High Resolution X-ray Diffractometry (HRXRD) measurements were performed at selected wafer areas, capturing the interplay between different dislocations or one specific dislocation type. The same defect types occur in all investigated wafers, namely Threading Screw Dislocations (TSD), Micropipes (MP), Small-angle grain boundaries (SAGB) in form of Threading Edge Dislocation (TED) arrays and Basal Plane Dislocations (BPD). Full wafer mappings, recorded in 0004 reflection show an inhomogeneous distribution of the mentioned defects (see Fig.1 (a) and (d)). In all wafer mappings, the defect density is lowest in the wafer center and increases towards the wafer border. The region between wafer middle and border is made up by a BPD network (see Fig.1 (b)), which corresponds to the crystal area with the highest calculated resolved shear stress distribution inherent during the growth temperature of 2250 °C [5]. In this area the shear stress exceeds a critical value for the formation of BPDs [6]. The network shows a connection to TSDs, whereas MPs are mostly isolated. Near the border there's a spontaneous change of the BPD network to an area of dominating SAGBs with a connection to MPs (see Fig. 1(c)). This change can be caused by a transition of BPDs into TEDs due to changing temperature and stress gradients during the cool down phase. By comparing the wafer close to the seed with the one close to the crystal cap, it becomes apparent that density, types and distribution of the occurring defects do not change along the crystal. Further, by using one wafer as seed for the next growth, defect types, density and distribution remains similar. Therefore, all types of threading dislocations and SAGBs continue during growth. HRXRD measurements were performed at different wafer areas to investigate the crystal quality more quantitatively. Rocking curves in 0004 reflection show a difference in their curve shape and full-width at half maximum (FWHM) depending on the crystal quality, which is in good agreement with the SWXRT results. More meaningful are the recorded Reciprocal Space Maps (RSM), to separate the effect of different defects on crystal lattice strain and tilt. Depending on the dominant defect type in the measured area the shape of the RSM and the relation of crystal lattice strain to crystal lattice tilt changes. A pure BPD network results in pure crystal lattice tilt, whereas mixed types of dislocation result in different amounts of strain and tilt. Even for the largest MPs, in combination with any type of edge dislocation, the contribution of pure lattice strain decreases. So in conclusion, there is no far-

reaching influence of one type of dislocations on the crystal lattice. Further, since most of the defects propagate through the whole length of the crystal, the crystal lattice strain and tilt conditions remain similar on the same wafer areas, irrelevant on the wafer position inside the crystal.

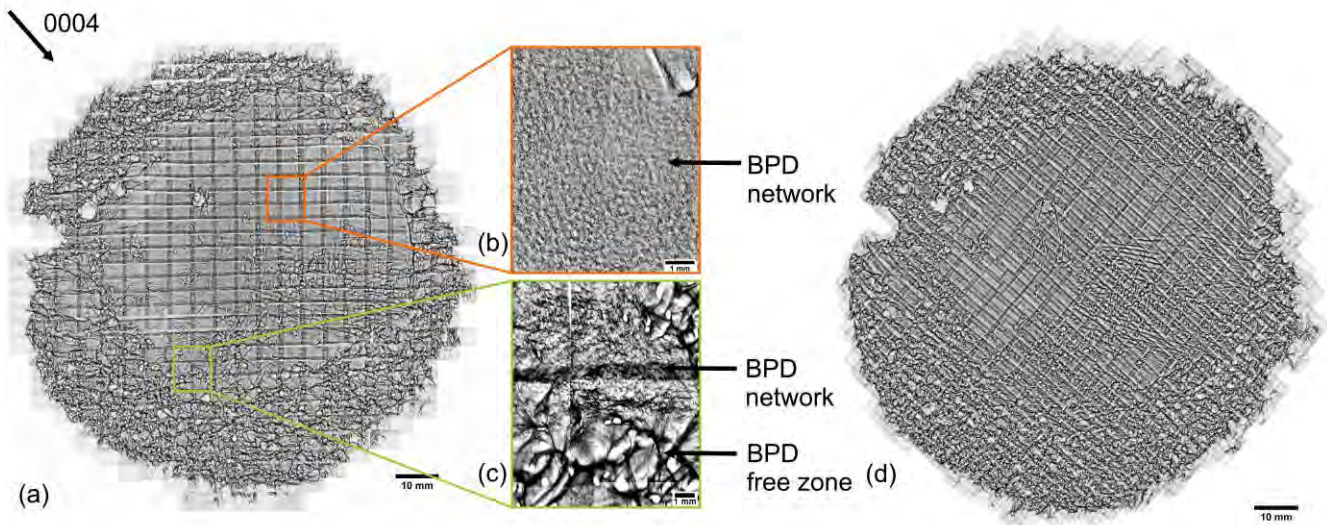


Fig. 1: (a) SWXRT wafer mappings recorded in 0004 of wafer A1, close to the crystal seed. (b) Circular arranged BPD network around the wafer center. (c) Abrupt transition from BPD network area to area with increased SAGBs. (d) SWXRT wafer mapping recorded in 0004 of wafer A2, close to the crystal cap. The mapping shows a similar defect arrangement as for wafer A1.

Acknowledgment

I want to thank our team at crystallography Freiburg. Mr. Harald Schade, Marcus Zuber and Elias Haman from KIT for technical support and all the help during beamtime and the "Deutsche Forschungsgemeinschaft" (DFG) for financial support, Project-Nr: 2083562101.

- [1] Neudeck, Ph G et al. "Breakdown degradation associated with elementary screw dislocations in 4H-SiC p+ n junction rectifiers." MRS Online Proceedings Library Archive 483 (1997).
- [2] Wellmann, P. J. et al. "Review of SiC crystal growth technology." Semiconductor Science and Technology 33.10 (2018): 103001.
- [3] Wellmann, P.J., et al. "Growth of SiC bulk crystals for application in power electronic devices—process design, 2D and 3D X-ray in situ visualization and advanced doping." Crystal Research and Technology 50.1 (2015): 2-9
- [4] Rack, A., et al. "The micro-imaging station of the TopoTomo beamline at the ANKA synchrotron light source." Nuclear Instruments and Methods in Physics Research Section B: Beam Interactions with Materials and Atoms 267.11 (2009): 1978-1988.
- [5] Steiner, Johannes, et al. "Analysis of the Basal Plane Dislocation Density and Thermomechanical Stress during 100 mm PVT Growth of 4H-SiC." Materials 12.13 (2019): 2207.
- [6] Selder, M., et al. "Numerical simulation of thermal stress formation during PVT-growth of SiC bulk crystals." Materials Science Forum. Vol. 353. Trans Tech Publications Ltd., Zurich-Uetikon, Switzerland, 2001.

Impact of Varying Parameters on the Temperature Gradients in 100 mm Silicon Carbide Bulk Growth in a Computer Simulation Validated by Experimental Results

J. Steiner^a, Matthias Arzig^a, Michael Salamon^b, Alexey Denisov^c, Norman Uhlmann^b,
Peter J. Wellmann^a

^a Crystal Growth Lab, Materials Science Department 6, Friedrich-Alexander-Universität Erlangen-Nürnberg, Martensstraße 7, 91058 Erlangen, Germany

^b Fraunhofer Institute for Integrated Circuits, Development Center for X-Ray Technology (EZRT), Flugplatzstraße 75, 90768 Fürth, Germany

^c PVA Crystal Growing Systems GmbH Im Westpark 10–12, 35435 Wettenberg, Germany
E-mail: johannes.steiner@fau.de

Summary

The extraordinary electrical properties of silicon carbide (SiC) established it as one of the currently relevant wide-band gap semiconductor materials for high power, high temperature, and high frequency electronic applications. Due to the increasing industrial standard size for SiC wafers from 100 mm up to 200 mm in the future, a fundamental understanding of the growth process and the corresponding conditions are crucial to achieve a crystal quality high enough for further processing. Commonly, SiC is grown by the physical vapor transport (PVT) method [1]. Changes of the growth conditions like axial and radial temperature gradients due to the growth of the SiC boule and shrinkage of the SiC source material lead to thermoelastic stresses and, as a result, defects are formed [2, 3]. The adaption of thermal gradients inside the hot zone is one way to reduce such defect generation. However, the high process temperatures prevent a straightforward in situ data acquisition from specific points inside of the crucible via thermocouples. Instead, numerical modeling can be used for hot zone engineering and to facilitate a better understanding of the complex dynamics during the PVT growth of SiC [4-6]. A major obstacle in the accurate modeling of the PVT growth process is the lack of precise material data at temperatures well above 2000°C of the applied carbon-based thermal isolations and crucible parts, as well as the highly dynamic SiC powder source. Moreover, material inhomogeneities can lead to further deviations of expected results. In this work, a quantification of the effects of these uncertainties on numerical modeling was done by utilizing the temperature data of growth runs inside a 75 mm PVT and two different 100 mm PVT setups and creating a simulation tool accurate enough to depict the process temperature fields with high accuracy covering a wide range of hot zone geometry and process parameters. Complementing X-ray imaging was done to characterize the evolution of crystal and source during the growth processes and further verify the numerical calculations [7, 8]. In addition, experimental validation was carried out by the comparison of simulated isothermals with experimental doping striations of the axial and radial temperature gradient and the evolution of the shape of the crystal growth interface (see fig. 1). This validated model enabled us to study the influence of changing materials properties of the graphite crucible, the SiC powder source or the graphite isolation on the accuracy of the simulation.

The impact of the cooling solution of a PVT setup either based on water or air on the temperature gradients inside the hot zone was investigated by growing two 100 mm crystals in two different PVT setups. It could be proved numerically and experimentally that the cooling solution has no influence on thermal gradients and the resulting crystals. Two additional 100 mm crystals were grown with varying source powder packaging densities. Using X-ray imaging, a correlation between the sources' packaging density and the curvature of the resulting crystal growth front could be demonstrated. Radial and axial temperature gradients will be influenced by the porosity of the source charge, as

validated by our model. Furthermore, the evolution of the source charge and its properties was investigated using an in situ CT-system. The insignificance of the source powder's electrical properties due to limited induction heating could be shown. While changing the thermal properties of the graphite hot zone will impact the radial gradient only to a minor degree, the axial gradients will be altered by a moderate amount. In case of unreliable thermal isolation material data the uncertainty can be lessened by adjusting the applied power in the simulation according to measured temperatures without losing too much accuracy. This however requires reliable temperature data on top and below the hot zone. Finally, the influence of the process pressure on the isolation has been investigated. The simulation is expanded by implementing a dependency between the pressure acting on the isolation and the resulting changes in thermal conductivity. With this implementation, the model can predict changes in temperature based on different growth pressures with high accuracy.

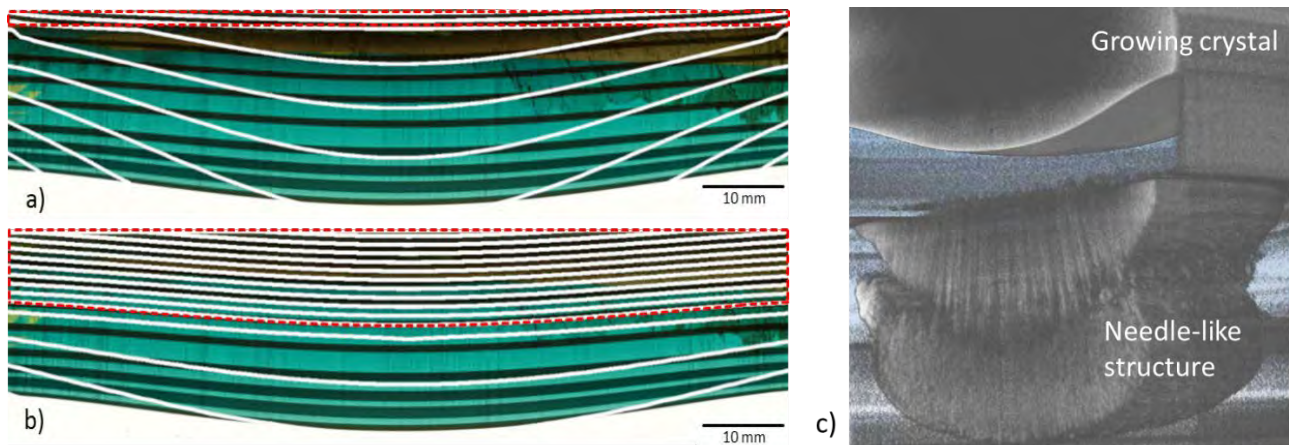


Fig. 1: Cross-section of a crystal grown with increasing power between 12.6 kW and 14.4 kW overlaid with isotherms derived from the simulation at a) the beginning of the growth and b) after 20 h growth. The seed and grown crystal is outlined in by the dashed line. c) In-situ 3D-CT-image of changing mass distribution inside the growth chamber.

Acknowledgment

The authors acknowledge funding by the DFG under the grant numbers WE2107/12-1 and UH246/4-1.

- [1] Y. M. Tairov, V. F. Tsvetkov, *Journal of Crystal Growth*, **43**, 209-212 (1978)
- [2] E. Schmitt, T. Straubinger, M. Rasp, A. D. Weber, *Superlattices and Microstructures*, **40**, 320-327 (2006)
- [3] D. Hofmann, E. Schmitt, M. Bickermann, M. Kölbl, P. J. Wellmann, A. Winnacker, *Materials Science and Engineering*, **61-62**, 48-53 (1999)
- [4] E. L. Kitanin, M. S. Ramm, V. V. Ris, A. A. Schmidt, *Materials Science and Engineering B*, **55**, 174-183 (1998)
- [5] M. Selder, L. Kadinski, Y. Makarov, F. Durst, P. Wellmann, T. Straubinger, D. Hofmann, S. Karpov, M. Ramm, *Journal of Crystal Growth*, **211**, 333-338 (2000)
- [6] D. D. Avrov, A. S. Bakin, S. I. Dorozhkin, V. P. Rastegaev, Y. M. Tairov, *Journal of Crystal Growth*, **198-199**, 1011-1014 (1999)
- [7] P. J. Wellmann, M. Bickermann, D. Hofmann, L. Kadinski, M. Selder, T. L. Straubinger, A. Winnacker, *Journal of Crystal Growth*, **216**, 263-272 (2000)
- [8] P. Wellmann, G. Neubauer, L. Fahlbusch, M. Salamon, N. Uhlmann, *Crystal Research and Technology*, **50**, 2-9 (2015)

NUMERICAL MODELLING OF THE CZOCHRALSKI GROWTH OF NEODYMIUM-SCANDATE SINGLE CRYSTALS

Klaus Böttcher, Wolfram Miller and Steffen Ganschow

Leibniz-Institut für Kristallzüchtung (IKZ) im FVB e.V., 12489 Berlin, Max-Born-Straße 2, Germany
E-mail: klaus.boettcher@ikz-berlin.de

NdScO₃ belongs to the group of the rare-earth scandates which has the perovskite structure. Concerning the lattice cell parameters, those rare-earth scandate perovskites meet other important perovskites, and so they are suitable substrates for the epitaxial growth of perovskite thin films because they are structurally, chemically and thermally compatible with them [1].

As most other perovskite-type rare-earth scandates, NdScO₃ melts congruently, NdScO₃ single crystals can be grown by the conventional Czochralski method with rf-heating and automatic diameter control. The most challenging property of NdScO₃ crystals is probably the semitransparency concerning internal radiative heat transfer.

In the present investigation, for solving of the heat transfer problem we have used the software CGSimTM [2] which is a tool for modelling crystal growth from the melt. For the solution of the radiative transport equation, CGSimTM uses a variant of the Discrete Transfer Method, that was adjusted to treat axisymmetric problems in complex domains, i.e. CGSimTM is able to solve the radiative transport equation for the full range of optical thickness.

Currently, NdScO₃ Czochralski crystals can be successfully grown up to a geometry of 45 mm length and 18 mm radius. However, from time to time they crack during wafer preparation, for that reason we are interested in the investigation of thermal stresses.

For treating the radiative heat transfer, as a first approach, we have defined different value ranges of a grey absorption coefficient μ in order to meet the various branches of the dimensionless optical thickness τ : for $\mu = 0.01 \dots 3 \text{ m}^{-1}$ we get $\tau < 0.1$, i.e. the medium is optical thin, for $\mu = 400 \dots 800 \text{ m}^{-1}$ we get $\tau > 10$, i.e. the medium is optical thick, and for $\mu = 10 \dots 200 \text{ m}^{-1}$, the medium is modelled as moderately optical thick.

The computations are performed in two steps: A: axisymmetric calculation of the temperature field in the entire furnace and of the field distribution of velocity for melt and gas using CGSim, whose algorithms performs power control in order that the temperature at the contact line between crystal, melt and gas keeps the melting point temperature and carries out the relocation of the finite-element mesh in order to track the shape of the crystal/melt interface. Then step B: from the crystal we take geometry and temperature field and expand them to 3D by rotating their data along 360 degree. This new data structure is put into software COMSOL[3]: now the anisotropic coefficients of thermal expansion and elasticity can take effect in order to make 3D displacements and thermal stresses in terms of the von Mises stress.

In Fig. 1 is shown the von Mises stress at the crystal surface for the 12 cases of absorption coefficients (ranging from optically thin via intermediate to thick). Additionally we see at the x-y line plots the deflections of the crystal/melt interface and the maximum values of the von Mises stress: we see that the cases with the largest stress values have intermediate absorption. Exactly these data sets have a similar deflection of the crystal/melt interface as in experiments: between 3 and 4 mm. This could explain the large residual stresses which lead to mechanical cracking at wafer preparation. For those cases (enboxed in Fig. 1) in Fig. 2 is shown the stress distribution within the crystals along a cross cut plane, for both cases: with and without the initial seed cone. The absence of the initial seed cone does not essentially change the thermal stress distribution near the crystal/melt interface.

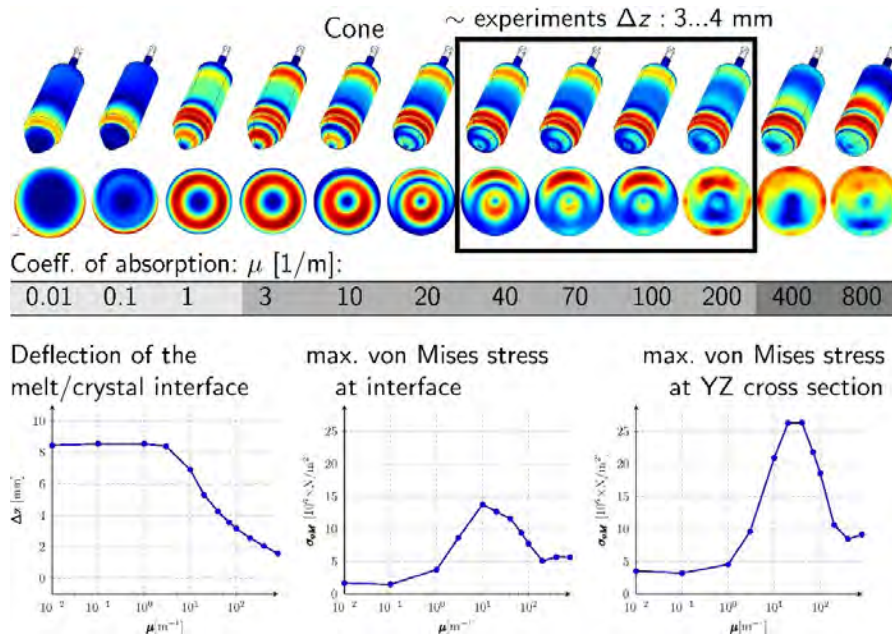


Fig. 1: Top: Von Mises stress at the crystal surface and at the crystal/melt interface (the circle below) as a result of the action of the absorption coefficient (see gray-scaled row from 0.01 ... 800 1/m), Bottom: Some results items in dependence of the absorption coefficient along the full range.

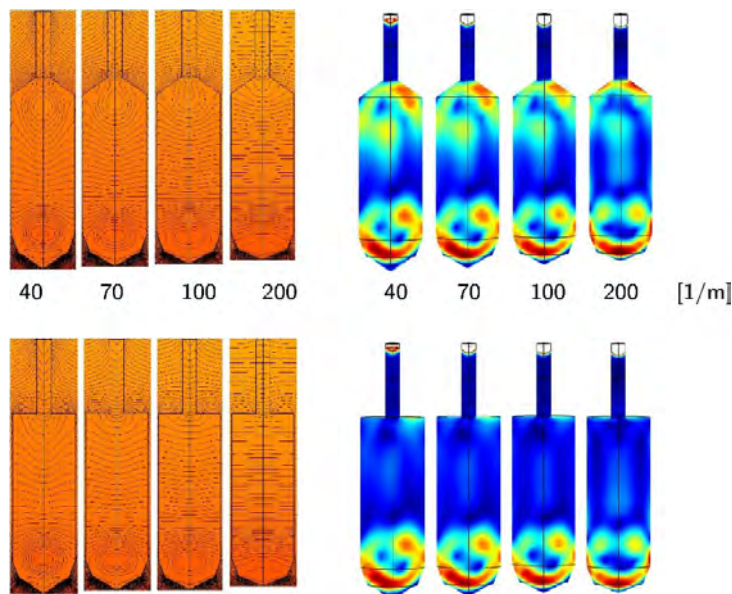


Fig. 2: Top: Temperature field and Von Mises stress at a crystal cross cut for the cases where the crystal/melt interface is in the range of the experimentally observed values:
 Top: Case with crystal conus after seed, bottom: Case without crystal conus after seed.

References:

[1] R. Uecker et al., Properties of rare-earth scandate single crystals (Re=Nd-Dy), Journal of Crystal Growth **310**, 2649-2658 (2008)
 [2] STR Group Inc.: CGSim Crystal Growth Simulator: Software for modelling of crystal growth from the melt, Theory manual (Ch. 7.1), Version 18.1, 2018, Saint Petersburg, Russian Federation.
 [3] Fa. COMSOL Inc.: COMSOL Multiphysics™, User Guide, Version 5.4, 2018, Burlington, USA.

Synthesis and characterization of the triangular antiferromagnets NaYbO₂, KYbO₂ and NaYbS₂

F. Grußler^a, P. Gegenwart^a, A. A. Tsirlin^a

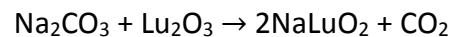
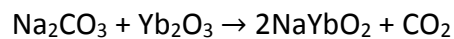
^a Experimental physics VI, Center for Electronic Correlations and Magnetism, University of Augsburg,
Augsburg, Germany.

E-mail: franziska.grussler@physik.uni-augsburg.de

Summary

NaYbO₂, KYbO₂ and NaYbS₂ feature the same space group $R\bar{3}m$ as the spin liquid candidate YbMgGaO₄ but evade structural disorder pertinent to that compound. Here, we present a way to synthesize polycrystalline NaYbO₂ and KYbO₂ as well as KYbS₂ single crystals.

The NaYbO₂ samples as well as the non-magnetic reference compound NaLuO₂ were synthesized via solid state reactions:



The precursors were weighed in the ratio of Na/Yb = 11. The excess of Na₂CO₃ is necessary, since at temperatures above 900°C some Na₂CO₃ is lost due to evaporation. They were pressed into pellets and subsequently heated according to the heating program shown in Fig. 1. Polycrystalline NaYbO₂ was synthesized by this method, no impurity phases were detected in synchrotron XRD measurements. Heat capacity measurements down to 100 mK in various magnetic fields revealed a field-induced order. Furthermore, spin-liquid behavior was demonstrated in NaYbO₂ [1].

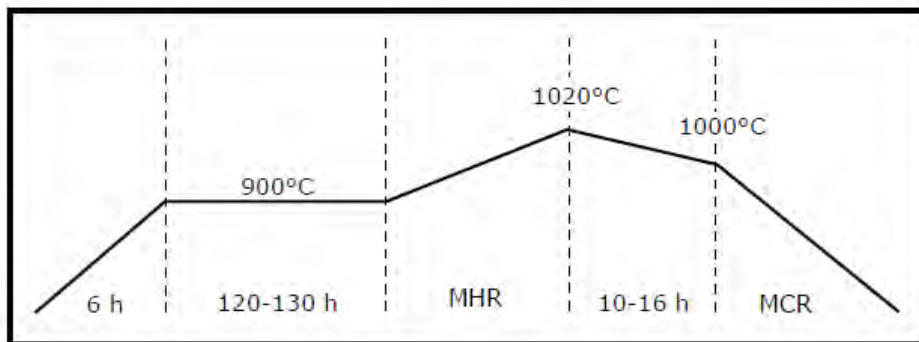


Fig. 1: Temperature profile used for the synthesis of NaYbO₂. The abbreviations MHR and MCR stand for the maximum heating rate and maximum cooling rate, respectively.

The approach of preparing KYbO₂ is based on the synthesis reported in [2]. The starting materials (Yb₂O₃ and KO₂) were weighed in a glove box filled with argon gas to prevent a reaction of KO₂ with the air moisture. As suggested in [2], an excess of KO₂ was used, the percentage of additional KO₂ was varied. In this case 75% additional KO₂ yields the best synthesis result. The precursors were filled into a platinum crucible and heated to 650°C in a horizontal furnace under argon flow. After the heat treatment the samples were stored in a glovebox under argon atmosphere since they are sensitive to the air moisture. XRD measurements revealed minor impurity phases of Yb₂O₃ and KOH·H₂O in the KYbO₂ samples.

KYbS₂ single crystals were synthesized using the KCl flux, with the ratio of Yb:S:KCl=2:3:80 [3]. S and KCl were weighed accordingly and thoroughly mixed in a mortar. Small pieces of Yb were placed in a quartz tube and covered with the S-KCl mixture. Subsequently, the precursors were sealed in the quartz tube under argon atmosphere. The sealed ampoule was placed in a furnace and heated in accordance to the heating program shown in Fig. 2 (left). Small KYbS₂ single crystals (<0.5mm) were formed shown in Fig. 2 (right). The success of the synthesis was verified via powder XRD measurements.

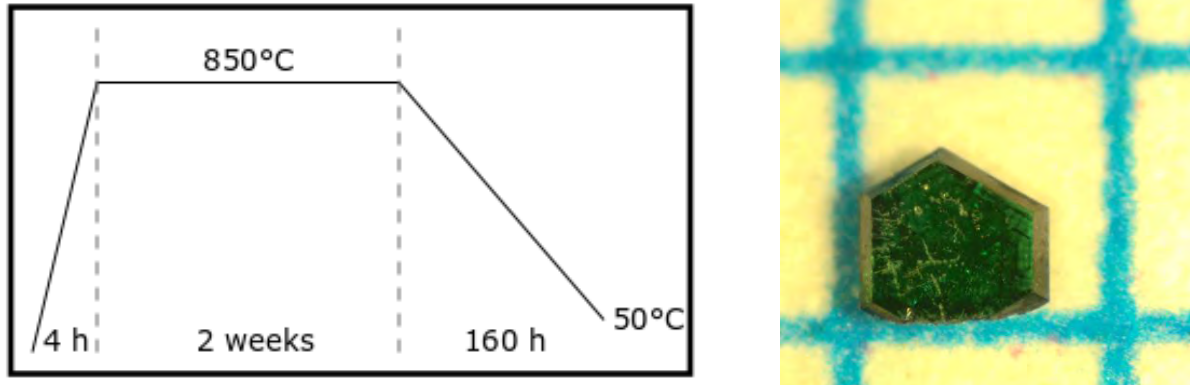


Fig. 2: Left: Temperature profile used for the synthesis of KYbS₂. Right: KYbS₂ single crystal.

Subject: Abstract Poster

- [1] L. Ding, P. Manuel, S. Bachus, F. Gräßler, P. Gegenwart, J. Singleton, R. D. Johnson, H. C. Walker, D. T. Adroja, A. D. Hillier, and Al. A. Tsirlin, *Physical Review B*, **100**, 144432 (2019)
- [2] B. Dong, Y. Doi, and Y. Hinatsu, *Journal of Alloys and Compounds*, **453(1)**, 282 – 287 (2008)
- [3] Ryosuke Iizaka et al. (Saitama University Japan)

The Influence of Sodium Dodecyl Sulfate on the Growth and Properties of Triglycine Sulfate Crystals

Ella Supik¹, Saskia Mihalic¹, Jannick Fammels¹, Rayhane Ghane-Motlagh²,
Peter Woias², and Andreas Danilewsky¹

¹ *Kristallographie, Institut für Geo- und Umweltnaturwissenschaften, Albert-Ludwigs-Universität Freiburg, Hermann Herder Str. 5, 79104 Freiburg, Germany*

² *Professur für Konstruktion von Mikrosystemen, Institut für Mikrosystemtechnik, Albert-Ludwigs-Universität Freiburg IMTEK, Georges-Köhler-Allee 102, 79110 Freiburg
E-mail: ellasusannsupik@googlemail.com*

Summary

This project investigates the influence of sodium dodecyl sulfate (SDS) on the morphology and structural properties of triglycine sulfate (TGS). TGS crystallises monoclinic in the space group $P2_1$ and shows a high pyroelectric effect parallel to the [010]-direction. The highest growth velocity of pure TGS is in the [010]-direction, as a result the (010)-faces disappear and will only appear as corners or edges. For a facilitated production of TGS infrared detectors the enlargement of the (010)-face is of great interest, if the pyroelectric figures of merit (FOM) are not heavily impacted.

J. Fammels [1] and S. Mihalic [2] started with several detergents to slow down the growth velocity in the [010]-direction. Sodium dodecyl sulfate (SDS) showed most promising results as described by R. Ghane [3,4]. The addition of SDS did not affect the pyroelectric coefficient (p_c) of 168 C/(m²K) at room temperature. However, the relative permittivity of 105 of TGS is decreased to 75 if SDS is added during growth. As a result, the figures of merit for voltage generation and for energy harvesting increased by 29 % to 201 kV/(mK) and 42,52 J/(m³K²) [4]. The pyroelectric coefficient was determined using a dynamic measuring method [3].

In this work a more suitable concentration of SDS was determined to further enlarge the (010)-face of the triglycine sulfate (TGS) crystals. Accordingly, the crystals were grown from aqueous solution with various concentrations of 0,00302 - 0,00306 Mol% of SDS, by the means of the temperature lowering method. The concentration of 552,04 g/l TGS resulted in a saturation temperature of 48,00 °C of the initial solution. The temperature was decreased at a rate of 0.08 °C/day, while continuously stirring with 60 rpm to ensure a homogenous concentration and temperature distribution during growth, without disturbing crystal growth. In all experiments, parasitic growth occurred on the bottom of the growth vessel, this however did not disturb the crystal growth. At higher concentrations of SDS (0.338 Mol% SDS), the parasitic crystals showed a needle-like structure [1,2], whereas parasites that formed during crystal growth of TGS with lower concentrations of SDS (<0.00306 Mol% SDS) showed a tabular habitus. The parasitic crystals were investigated and compared by the means of X-ray-powder-diffraction (XRD). The powder diffractometry of pure TGS, the tabular and needle shaped parasites show entirely different results. This leads to the assumption that the parasites are composed of different substances than TGS, the substance has not been identified yet.

One of five crystals, grown from solutions with low concentrations of SDS (<0.00306 Mol% SDS) developed monocrystalline (Fig. 2) with clear and well-developed faces, whereas four crystals started twinning (Fig. 1) in the course of the growth process. The twinning was initiated by sudden temperature changes and oversaturation of the solution and caused an acceleration of growth in [010]-direction. Thus, the (010)-face did not develop in the twinned crystals as shown in Fig. 1. Assuring a stable temperature reduction of 0.08 °C/day prevents the crystals from twinning.

Accordingly, monocrystalline TGS crystals with an enlarged (010)-face can be produced. The addition of 0,00306 Mol% SDS caused the largest reduction of growth velocity in [010]-direction. A monocrystalline crystal with a large (010)-face resulted, as shown in Fig. 2. The grown crystals were characterized by Laue measurements and X-ray-powder diffraction (XRD). The XRD analysis did not show any changes compared to pure TGS. Furthermore, IR-spectra of TGS crystals grown with 0,39 Mol% SDS, show the same peaks as pure TGS, thus no incorporation of SDS in the TGS crystals occurs [4].

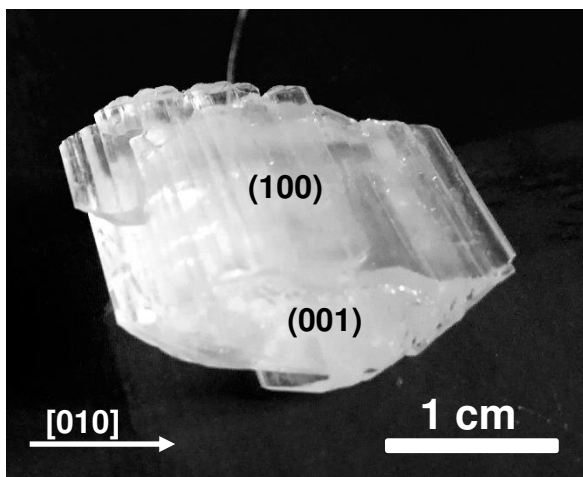


Fig. 2: Twinned TGS crystal grown with 0,00304 Mol% SDS. The twinning plane is parallel to the (100)-face.

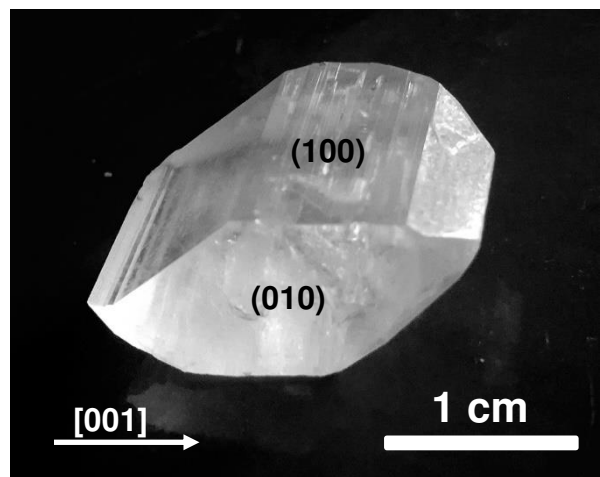


Fig. 2: Monocrystalline TGS crystal grown with 0,00306 Mol% SDS. The crystal inhibits a large (010)-face.

Acknowledgment

The authors thank Otto Schäfer, Müllheim for helpful discussions.

- [1] J. Fammels, BSc-thesis Albert-Ludwigs-Universität Freiburg, (2017), unpublished.
- [2] S. Mihalic, BSc-thesis Albert-Ludwigs-Universität Freiburg, (2019), unpublished.
- [3] R. Ghane-Motlagh, M. Kroener, F. Goldschmidtboeing, A.N. Danilewsky, P. Woias, Smart Mater. Struct. 27 (2018), 084004.
- [4] R. Ghane-Motlagh, J. Fammels, A. N. Danilewsky, U. Pelz, and P. Woias, J. Crystal Growth & Design, (2020), submitted.

Single-crystal growth and magnetic phase diagram of TbFeO₃

Alexander Engelhardt^a, Georg Benka^a, Andreas Bauer^a, Andreas Erb^b, Christian Pfleiderer^a

^a Fakultät für Physik, Technische Universität München, James-Franck-Straße 1,
85748 Garching, Germany

^b Walther-Meißner-Institut, Bayerische Akademie der Wissenschaften, Walther-Meißner-Straße 8,
85748 Garching, Germany
E-mail: alexander.engelhardt@tum.de

Summary

The results are presented of the experimental investigation of the magnetic properties of the orthorhombic perovskite TbFeO₃. This compound has two magnetic sublattices resulting in complex magnetic phases. Furthermore, using neutron diffraction it was shown that it hosts a magnetic soliton lattice, a complex and anharmonic magnetic structure [1]. In the presented work, single crystal TbFeO₃ was synthesized by means of a combination of a solid-state reaction and the optical floating zone technique. X-ray powder diffraction patterns recorded at different temperatures revealed an anomaly in the thermal expansion at the antiferromagnetic ordering temperature of the iron spins at $T_N = 688$ K. Measurements of the zero-field magnetic susceptibility and of the heat capacity between 2 K and 300 K revealed the presence of two magnetic phase transitions, namely a ordering of the terbium spins around 8 K and a spin-reorientation of the two magnetic sublattices around 3 K. Based on measurements of the longitudinal ac susceptibility, various magnetic spin configurations were identified in detailed phase diagrams at low temperatures for magnetic fields applied along the three major crystallographic axes of the orthorhombic system. The main result, in particular, concerned the observation of the soliton lattice state by means of measurements of the transverse susceptibility when the external magnetic field is applied along the c-axis.

Acknowledgment

We wish to thank Andreas Erb and Astrid Habel for the supervision during the preparation of polycrystalline oxide rods for the optical floating zone technique. We acknowledge Susanne Mayr for the preparation of oriented single crystals. Financial support was provided through DFG TRR80.

[1] S. Artyukhin, M. Mostovoy, Nature Materials, **11**, 694-699 (2012)

Crystalgrowth of Fe-doped Li_3N

F. Breitner^a, M. Fix^a and A. Jesche^a

^aEP VI, Electronic Correlations and Magnetism, University of Augsburg, Germany
E-mail: franziska.breitner@physik.uni-augsburg.de

Summary

$\text{Li}_2(\text{Li}_{1-x}\text{Fe}_x)\text{N}$ shows fascinating magnetic properties with high magnetic anisotropy and huge hysteresis. The spin reversal is dominated by quantum tunneling of the magnetization and the system can be considered a single atom magnet [1]. Here, we present a method for growing $\text{Li}_2(\text{Li}_{1-x}\text{T}_x)\text{N}$ single crystals doped with iron and other transition metals $T = \{\text{Mn}, \text{Co}, \text{Ni}, \text{Cu}\}$ from a lithium-rich melt. Liquid lithium has a low melting point as well as a high solubility for nitrogen already at comparatively low temperatures of 800°C and below [2]. The low solubility of transition metals in pure lithium can be considerably improved by adding a third element, in this case nitrogen. Both these properties make lithium a promising flux for the growth of nitride-based single crystals.

Crystal growth of $\text{Li}_2(\text{Li}_{1-x}\text{T}_x)\text{N}$ is performed using a three-cap-crucible which is made from a niobium tube, two caps and a strainer also made from niobium. Due to the high reactivity of lithium and the air and moisture sensitivity of the reactants and the final product, all manipulations were carried out in an argon-filled glovebox (with O_2 and H_2O below 0.5 ppm). After loading the starting materials (Li, Li_3N and T), the crucible is sealed by welding the cap to the tube using an arc-melter. This crucible is again sealed in a quartz ampoule under argon atmosphere to prevent the niobium from oxidation and placed in a furnace. The mixture is then heated to a maximum temperature of 850°C, cooled down to 750°C within an hour and slowly cooled down to 500°C over typically 150 hours. After the growth process is finished, the crystals are separated from the flux via high temperature centrifugation which is performed within seconds after the sample has been removed from the furnace at 500°C [3].

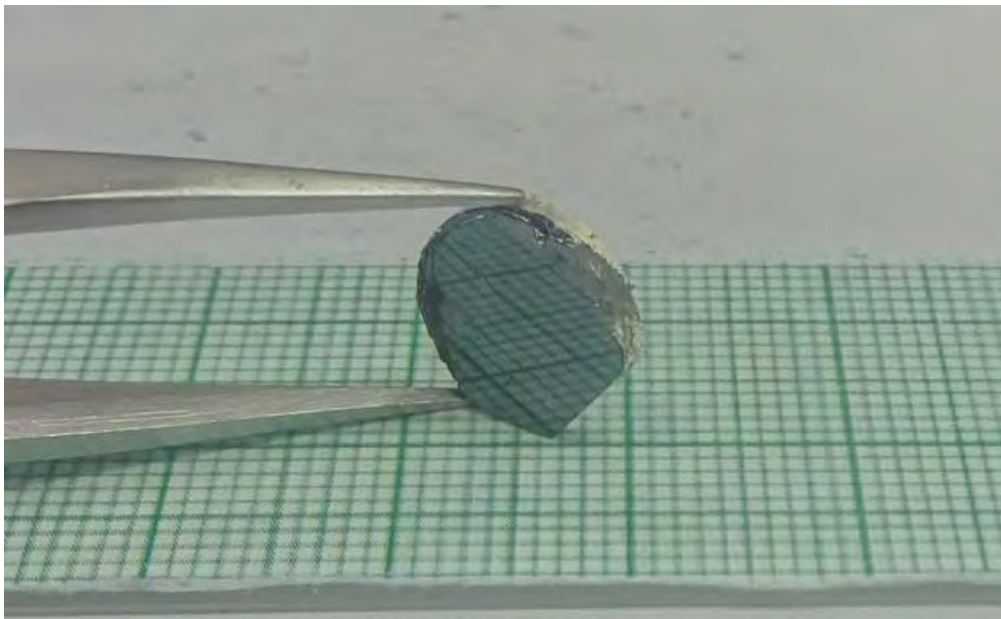


Fig. 1: As-grown Li_3N single crystal obtained from lithium-rich flux on a millimeter grid.

The obtained single crystals show a hexagonal symmetry and a side length of several millimeters. In some cases, the size of the crystals is limited by the diameter of the used niobium crucible of 12mm. A significant amount of lithium in the crystals grown using this method can be substituted with transition metals, e.g. $x = 30 \%$ for $T = \text{Fe}$. The habit and size of the resulting crystals are significantly influenced by the introduction of the different transition metals. Structural characterization was performed using X-Ray diffraction and chemical analysis by means of inductively coupled plasma optical emission spectrometry measurements.

The size and quality of the single crystals allow for a plethora of experiments to be performed such as measurements of the anisotropic magnetic, thermodynamic and optical properties.

Acknowledgment

This work was supported by the Deutsche Forschungsgemeinschaft (DFG, German Research Foundation) - Grant No. JE748/1.

- [1] M. Fix, J.H. Atkinson, P.C. Canfield, E. del Barcon, and A. Jesche, Phys. Rev. Lett. **120**, 147202 (2018)
- [2] T. Massalski, Binary Alloy Phase Diagrams, Volume **3**, 2448 (1990)
- [3] A. Jesche and P. Canfield, Phil. Mag. **94**, 2372-2402 (2014)

Microstructural evolution of intermetallics under the influence of magnetic field annealing – exemplified by Mn_3Ga

G. Kirste^a, C.G.F. Blum^a, J. Freudenberger^a, S. Wurmehl^a, B. Büchner^a

^a Leibniz-Institut für Festkörper- und Werkstoffforschung, Helmholtzstraße 20, 01069 Dresden, Germany

E-mail: g.kirste@ifw-dresden.de

Summary

Magnetic field annealing is a valuable tool for influencing microstructure and texture. The origin of this approach lies within the interaction of an external magnetic field with the sample's magnetic anisotropy. Although anisotropic magnetic susceptibility may even be found in diamagnetic materials, magnetic field annealing is especially interesting for materials with exceptional ferromagnetic properties. Among these materials with high response to external magnetic fields are Heusler related intermetallics - like Mn_3Ga , showing a $D0_{22}$ structure.

The Mn-Ga phase diagram being rather complex, this phase cannot be obtained by a simple melting process. In such cases magnetic field annealing provides another advantage. With the aid of the magnetic contribution to Gibbs free energy the applied external magnetic field may act as key to promoting phase formation or even enable new phase formation routes. For Mn_3Ga , *Ener et al.* depicted the magnetic field-assisted formation of the $D0_{22}$ phase [1].

Referring to those previous findings, Mn_3Ga samples were annealed for up to two weeks within this study. The results of conventional annealing were contrasted with those of magnetic field annealing in a superconducting magnet using a magnetic flux density of 7 T (*Figure 1*). Beforehand the arc melted samples received rotary swaging to increase the defect concentration, which further forwards the phase transformation. In the course of characterization, we focused on the progression of microstructure using microscopical methods, supplemented by some analysis via X-ray diffraction and SQUID magnetometry.

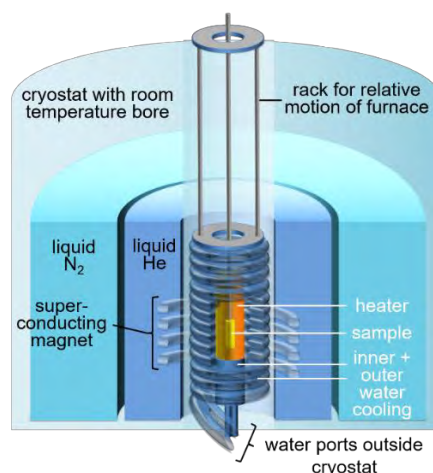


Fig. 1: Experimental setup for magnetic field annealing in a superconducting magnet.

The achieved differences in microstructural evolution with and without application of an external magnetic field will be discussed. Furthermore, the example of Mn_3Ga will be used to sketch the capabilities of magnetic field processing for tailoring the microstructure of intermetallics in general.

References

- [1] S. Ener, K.P. Skokov, D.Y. Karpenkov, M.D. Kuz'min, O. Gutfleisch, *Journal of Magnetism and Magnetic Materials*, **382**, 265-270 (2015)

ZF NMR AS A TOOL TO CLARIFY CRYSTALLOGRAPHIC, MAGNETIC AND ELECTRONIC STRUCTURE OF MAGNETICALLY ORDERED MATERIALS

P.Fritsch^a, F. Hammerath^a, J. Lucassen^b, C. F Schippers^b, M. A. Verheijen^{b,c}, E. J. Geluk^d, B. Barcones^d, R. A. Duine^{b,e}, H. J. M. Swagten^b, B. Kopmans^b, R. Lavrijsen^b, S.Wurmehl^{a,f}

^a IFW Dresden, Institute for Solid State Research, Helmholtzstraße 20, 01069 Dresden, Germany

^b Department of Applied Physics, Eindhoven University of Technology, P.O. Box 513, 5600 MB Eindhoven, the Netherlands

^c Eurofins Materials Science BV, High Tech Campus 11, 5656 AE Eindhoven, The Netherlands

^d NanoLab@TU/e, Eindhoven University of Technology, P.O. Box 513, 5600 MB Eindhoven, the Netherlands

^e Institute for Theoretical Physics, Utrecht University, Princetonplein 5, 3584 CC Utrecht, the Netherlands

^f Institute of Solid State and Materials Physics, TU Dresden, 01062 Dresden, Germany

E-mail: p.fritsch@ifw-dresden.de

Macroscopic properties of (magnetically ordered) materials are inseparably linked to their (local) structure. Hence, any specific functionality can only be understood and tailored if the structure-property relationships are taken into account.

Nuclear magnetic resonance spectroscopy (NMR) is a known standard technique for structure analysis on a wide range of materials. The basis of NMR is the interaction of the nucleus' spin with an external magnetic field, neighboring nuclei and the surrounding electrons. The externally applied field is the determining factor in paramagnetic and diamagnetic matter. However, for magnetically ordered materials the strongest contribution stems from the hyperfine field originating in the hyperfine interaction of the nuclear magnetic moment with the magnetic field deriving from the spin and orbital currents of the surrounding electrons. Therefore magnetically ordered materials can be probed with ease under zero external field. Zero-field nuclear magnetic resonance spectroscopy (ZF NMR) is a tool to probe the local environment of the NMR active nuclei on an integral scale. This tool enables a variety of local properties, such as local crystallographic defects, lattice strain, magnetic stiffness, local magnetic moments and even the local electronic structure [1-3].

We use ZF NMR to investigate Co thin films with the different thicknesses $t = 10$ nm and $t = 25$ nm. The objective in this work is to explain the increase in magnetic anisotropy with increasing film thickness [4]. The investigation with ZF NMR as a local probe gives us information about the ratio and magnetic stiffness of different crystallographic phases and stacking faults present in the films. Figure 1 shows the ⁵⁹Co ZF NMR spectrum for the sample $t = 25$ nm. The spectrum is fitted with an appropriate Gaussian model to extract the exact resonance frequencies of each specific crystallographic environment and their corresponding ratio in the overall film. The resonance frequencies are compared with the literature and assigned accordingly [5]. Two allotropes can be found within the thin film: fcc (blue line) and hcp (magenta line). While hcp Co is the stable allotrope under ambient condition, Co grows in the fcc structure on top of Pt due to lattice mismatch. Between the fcc and hcp environment two distinguishable stacking fault (sfs) environments can be found. Concerning the magnetic anisotropy and how this is linked to the structural finding, there are two possible sources for the increase in this property. Either the observed magnetic anisotropy stems from a magnetocrystalline (intrinsic) effect due to the larger contribution of hcp Co in the thicker film which is inherently more anisotropic than fcc Co or the anisotropy originates in the magnetoelastic (extrinsic) effect, due to defect pinning on the sites of the stacking faults between the fcc and hcp Co. We will

give an answer to this question as well as more examples from our recent research underlining the potential of ZF NMR to understand structure-property relationships in modern materials.

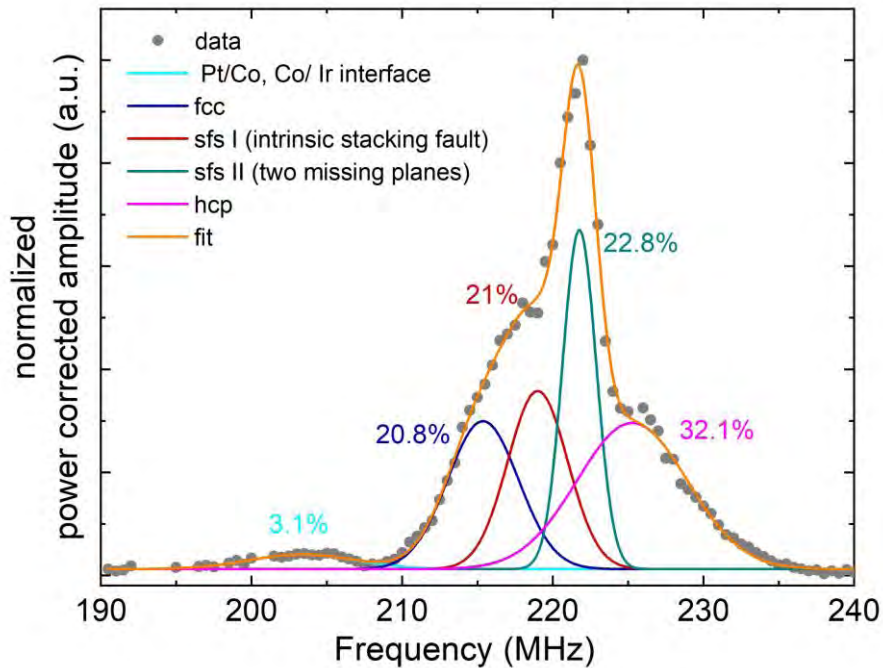


Fig. 1: ^{59}Co ZF NMR frequency spectrum of a Co thin film (thickness $t = 25$ nm).

Acknowledgment

Financial support is acknowledged from the Deutsch Forschungsgemeinschaft (DFG) through Grants No. WU595/3-3 and WU595/14-1

- [1] A. C. Gossard and A. M. Portis, Phys. Rev. Lett., **3**, 164 (1959)
- [2] P. Panissod and C. Mény, Appl. Magn. Reson., **19**, 447-460 (2000)
- [3] S. Wurmehl and J. T. Kohlhepp, J. Phys. D: Appl. Phys., **41**, 173002 (2008)
- [4] J. Lucassen, C. F. Schippers, M. A. Verheijen, P. Fritsch, E. J. Geluk, B. Barcones, R. A. Duine, S. Wurmehl, H. J. M. Swagten, B. Koopmans, R. Lavrijsen, arXiv:1909.02467, (2019)
- [5] G. J. Strijkers, J. T. Kohlhepp, H. J. M. Swagten, W. J. M. de Jonge, Appl. Magn. Reson., **19**, 461-469 (2000)

LnMn₂Ge₂ (Ln = Nd, Sm, Dy): SINGLE CRYSTAL GROWTH AND CHARACTERIZATION

K. Kliemt, M. Ocker, R. Möller and C. Krellner

Kristall- und Materiallabor, Goethe-Universität Frankfurt, Max-von-Laue-Str.1, 60438 Frankfurt, Germany
kliemt@physik.uni-frankfurt.de

Among the 122 compounds which crystallize in the ThCr₂Si₂-type structure, the compounds LnMn₂Ge₂, where Ln is a rare earth element, stand out since they exhibit a complex magnetic behaviour. At high temperatures, the magnetism is dominated by the ordering of the 3d electrons of Mn, while at low temperatures it is determined by the ordering of the rare earths local moments [1, 2].

There are many studies of polycrystalline samples or small single crystals, but large and pure single crystals suitable for spectroscopic studies are missing. In previous work, the possibility of the growth of single crystals from indium flux was reported [3]. Our attempts to grow the LnMn₂Ge₂ (Ln=Nd, Sm, Dy) from indium or tin flux failed. Instead, we succeeded to grow these compounds from a stoichiometric mixture of the elements.

In this contribution, we present the details of the growth by Czochralski method. Preliminary differential thermal analysis (DTA) showed that the compounds do not grow congruently. Furthermore it turned out that the evaporation of Mn from the stoichiometric melt is considerably large. Therefore, we applied the Czochralski method using a levitating melt under enhanced Ar pressure for the growth (Fig. 1, left). Recently, this procedure was developed and successfully applied to the single crystal growth of the ferromagnetic quantum-critical compound YbNi₄P₂ [4]. From the grown samples, mm-sized single crystals of LnMn₂Ge₂ were extracted (Figs. 2 and 3). In this contribution, we will present the chemical and structural characterization of the Czochralski grown LnMn₂Ge₂ crystals and some physical measurements around the magnetic transitions.



Fig. 1: *Left*: Crystal growth by Czochralski method from a levitating melt. *Right*: ThCr₂Si₂-type structure of the LnMn₂Ge₂ compounds.

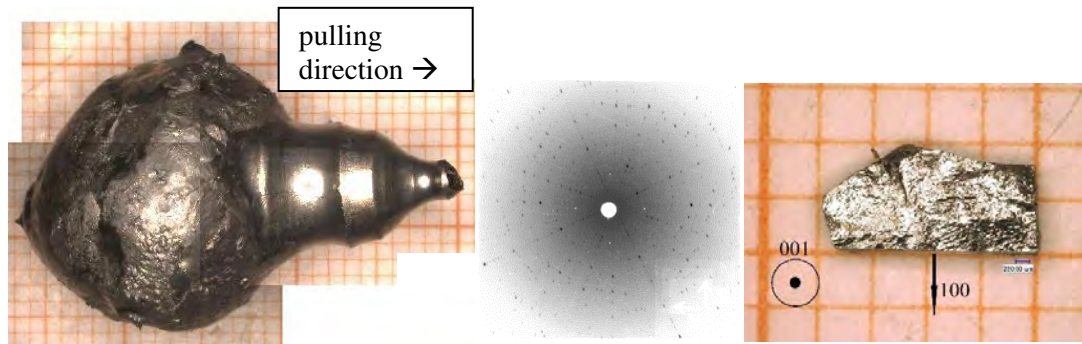


Fig. 2: *Left*: SmMn₂Ge₂ Czoehrski grown sample. *Middle*: Laue pattern view along the tetragonal axis. *Right*: Extracted single crystal grain of SmMn₂Ge₂.

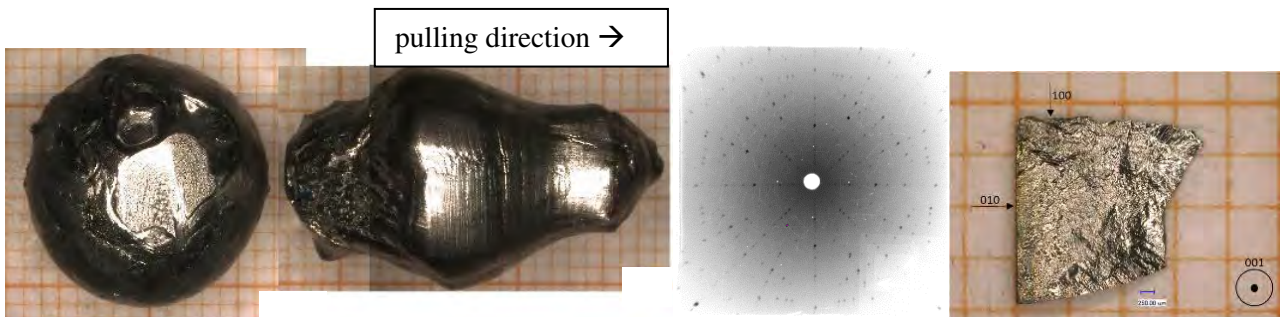


Fig. 3: *Left*: NdMn₂Ge₂ Czoehrski grown sample separated from the residual flux. *Middle*: Laue pattern, view along the tetragonal axis. *Right*: Extracted single crystal grain of NdMn₂Ge₂.

- [1] G. Guanhua et al., Journal of Experimental and Theoretical Physics 93, 796 (2001).
- [2] N. P. Kolmakova et al., Low Temperature Physics 28, 653 (2002).
- [3] E. M. Gyorgy et al., Journal of Applied Physics 61, 4237 (1987).
- [4] K. Kliemt, C. Krellner, J. Cryst. Growth 449, 129 (2016).

Directly analyzing the depth dependent properties of Cu(In,Ga)(S,Se)₂ wedges manufactured by exfoliation and a nontoxic, adjustable etching process

M. Schuster^a, U. Künecke^a, P.I. Reyes Figueroa^b, R. Klenk^b, P.J. Wellmann^a

^a Institut Materialien der Elektronik und der Energietechnologie (i-MEET), Friedrich-Alexander Universität, Martensstr. 7, 91058 Erlangen, Germany

^b PVcomB, Helmholtz Zentrum Berlin (HZB), Hahn-Meitner-Platz 1, 14109 Berlin, Germany
E-mail: msc.matthias.schuster@fau.de

Summary

The material system of Cu(In,Ga)(S,Se)₂ (CIGS) is well-established among high efficiency thin film solar cells. The physical properties of CIGS throughout the absorber layer depend on the depth distribution of composition profiles, especially elemental profiles of Ga and S. Thus a reliable quantification technique is required, especially to tune the optoelectronic properties like the band gap energy. In this work a nontoxic and adjustable etching process was used to prepare wedge-shaped samples for further direct analysis – both from CIGS absorbers on glass substrates (provided by Helmholtz Zentrum Berlin) as well as from exfoliated CIGS films. Large area energy dispersive X-ray spectroscopy (EDX) with different acceleration voltages from the front (CIGS on substrate) and from the back side (exfoliated CIGS film) was used to acquire a first determination of the element composition. The CIGS wedges were characterized by field emission scanning electron microscopy (FESEM) to evaluate the morphology, EDX at 10 kV to determine the local element composition and distribution, and photoluminescence (PL) to investigate the optoelectronic properties. A schematic of the sample preparation and characterization processes can be seen in Fig.1.

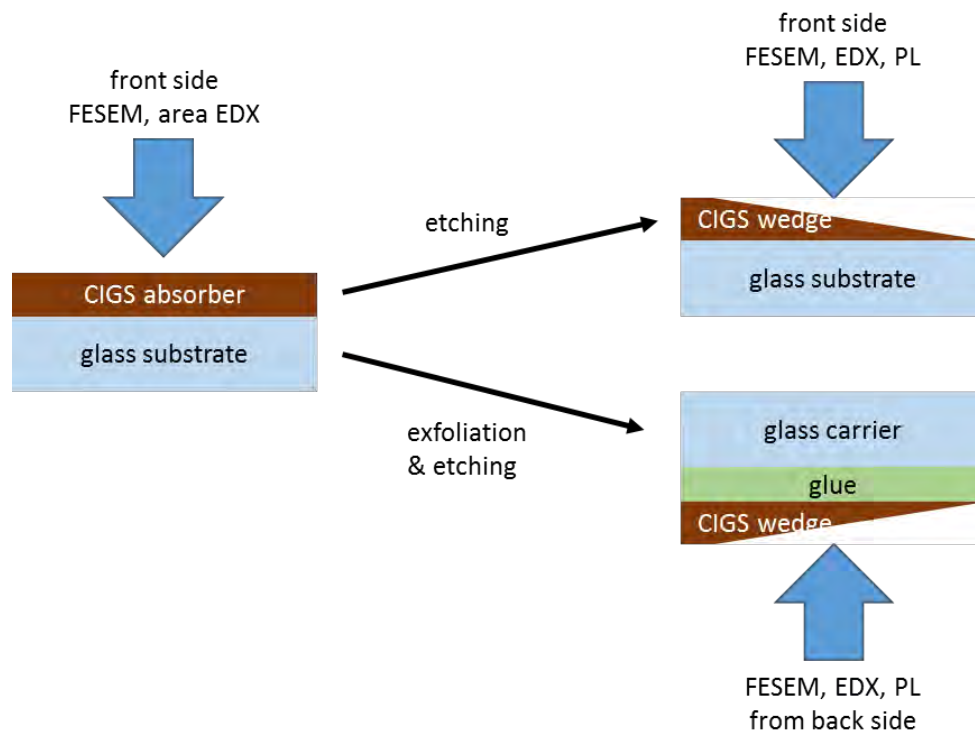


Fig. 1: Schematic of the CIGS wedge sample preparation and the performed characterization measurements.

In Fig.2 the different sample types are compared concerning their Cu(In+Ga) and Ga(In+Ga) ratios as well as their Sulfur and Selenium content throughout the CIGS film. The respective amounts were measured by area EDX with different acceleration voltages from the front side and the back side. After etching the CIGS on substrate and exfoliated CIGS films, low voltage EDX measurements are used to further analyze and confirm the expected elemental profiles.

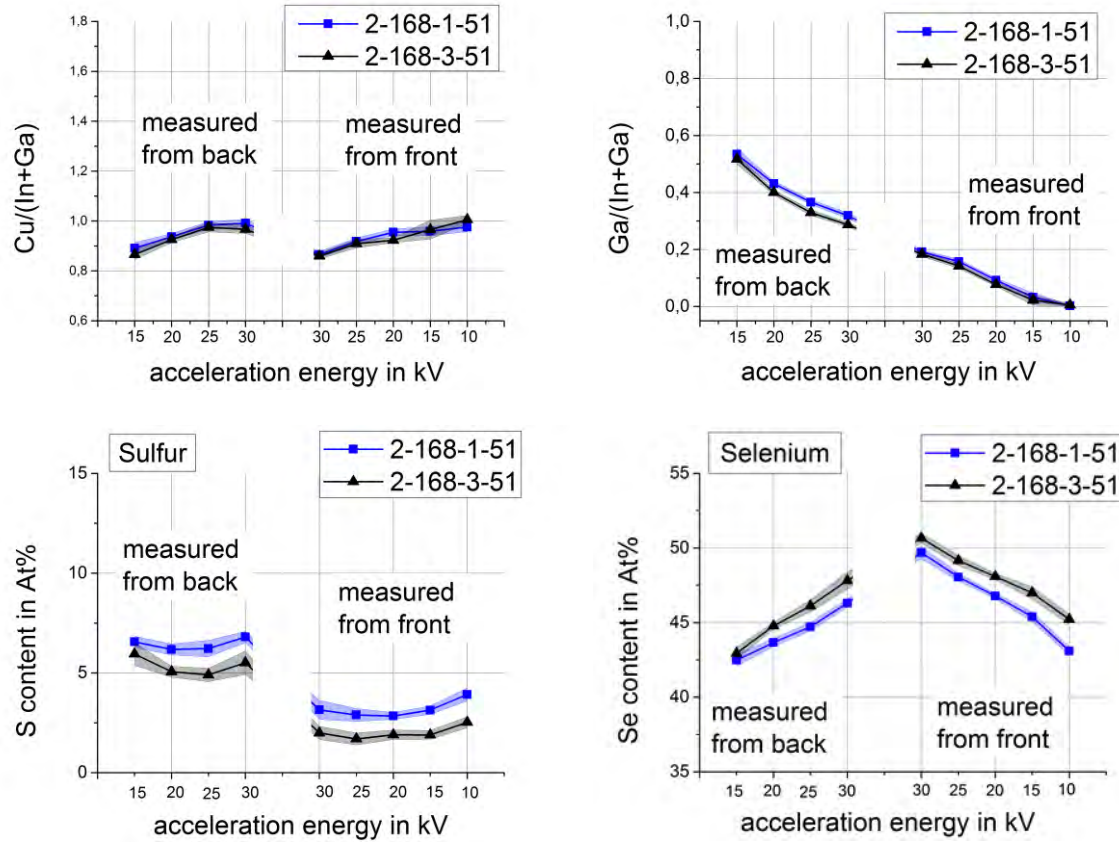


Fig. 2: Values of Cu(In+Ga), Ga(In+Ga) and S content throughout the layer as measured with area EDX with different acceleration voltages from the front (CIGS on substrate) and from the back (exfoliated CIGS films).

The directly measured (PL) minimum band gap energy is slightly lower than the estimated value from the composition gradients that were measured by glow discharge optical emission spectroscopy (GDOES). Moreover throughout the CIGS film a rise in band gap energy can be measured, as the amount of Ga increases towards the back contact.

Acknowledgment

The authors thank Erik Waack and Ralf Haberecht from HZB for providing the CIGS films. This project is funded under support code 0324154 by the German Ministry of Economic Affairs and Energy (BMWi) on the basis of a decision by the German Bundestag.

Crystal growth of (Cd,Zn)Te under microgravity Vampir-F: Characterization of ground experiments

J. Zou¹, A. Fauler¹, A.S. Senchenkov², N.N. Kolesnikov³, M. Fiederle¹

¹ Materials Research Center FMF, Freiburg, Germany

² Research and Development Institute for Launch Complexes NIISK, Moscow, Russia

³ Institute of Solid State Physics of Russian Academy of Sciences, Chernogolovka, Russia

E-mail: jiaona.zou@fmf.uni-freiburg.de

Cadmium zinc telluride ((Cd,Zn)Te) has been considered a promising material for the fabrication of room temperature X- and Gamma-Ray detectors, owing to its excellent electrical properties and its high density. Travelling Heater Method (THM), which is a solution growth technique, allows the preparation of monocrystalline material with the required electrical properties regarding high resistivity and high carrier mobility-lifetime-products. The THM method provides a uniform crystal composition of ternary materials such as (Cd,Zn)Te.

Nevertheless, the application is limited by the presence of material defects, such as Te inclusions, twins and even cracks. The growth of defect-free quality (Cd,Zn)Te crystals still remains a challenge. Microgravity conditions provide unique possibilities to improve the quality of the crystals owing to suppression of buoyancy convection. To study the influence of microgravity on the crystal quality, two space experiments 'VAMPIRE-F' are scheduled for 2021. The preparation of these experiments includes the growth of several crystals using THM and the characterization of these crystals as well as the growth of seed material in our 3 inch THM facility.

Some of the important parameters of the ground experiments are shown in Tab. 1. After performing the first two ground experiments, two problems have been found. Firstly, there was a large zinc concentration variation at the boundary between the seed and the grown crystal. And secondly, both of the seeds were almost not dissolved. Therefore, some parameters have been adjusted for the third experiment aiming to solve these problems. First, the CdTe concentration in the Te Zone was increased from 5 % to 10 %. In addition, the heater temperature at the beginning of the translation was increased and then went back slowly. At last, the starting position of the heater was moved 5 mm towards the seed direction.

Tab. 1: experimental parameters of the three ground experiments

sample No.	doping	CdTe % in Te Zone	heater temperature	RMF	heater position
F1-01-GM	In (5 ppm)	5%	1080-1100 °	no	Zone centre
F1-02-GM	In (5 ppm)	5%	1100-1110 °	2 mT, 100 Hz	Zone centre -2 mm
F1-03-GM	In (5 ppm)	10%	1110-1100-1110 °	2 mT, 100 Hz	Zone centre -5 mm

In this study, Infrared Transmission Microscope was used to analyze the defects distribution, like Te inclusions. Birefringence measurement and optical microscopy were performed to analyze the stress distribution in the crystals. Further, X-ray Diffraction (XRD) and Energy Dispersive X-ray Spectroscopy (EDX) were done to obtain further information of the Zn concentration and defects in the crystals. In addition, Contactless Resistivity Mapping (COREMA) was used to measure the resistivity of the crystals.

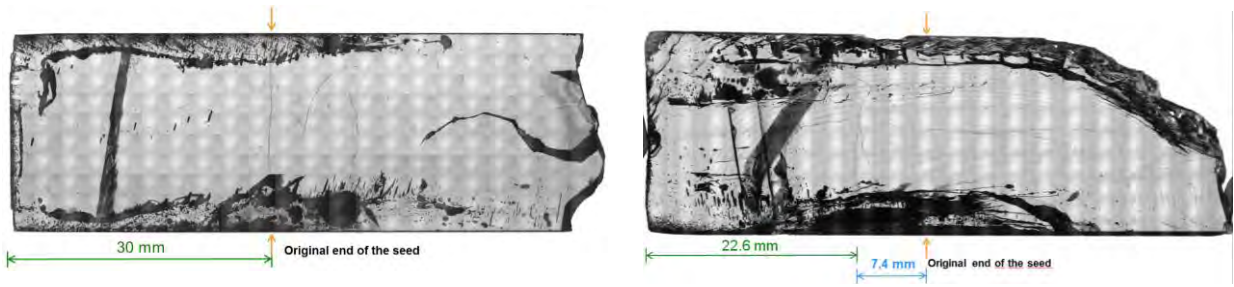


Fig. 1: IR images of F1-02-GM (left) and F1-03-GM (right). The seed of the second sample F1-02-GM was not dissolved, while the seed of F3-03-GM was dissolved for 7.4 mm after adjustment of the experimental parameters.

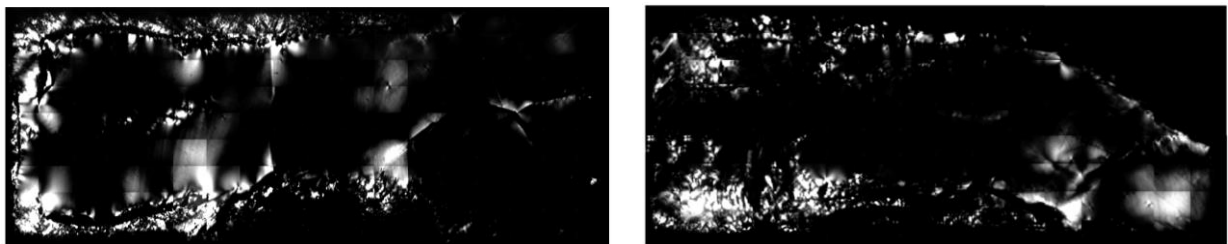


Fig. 2: Birefringence mappings of F1-02-GM (left) and F1-03-GM (right). Some stress was found at the boundary of F1-02-GM, while the boundary of F1-03-GM is free from dramatic stress.

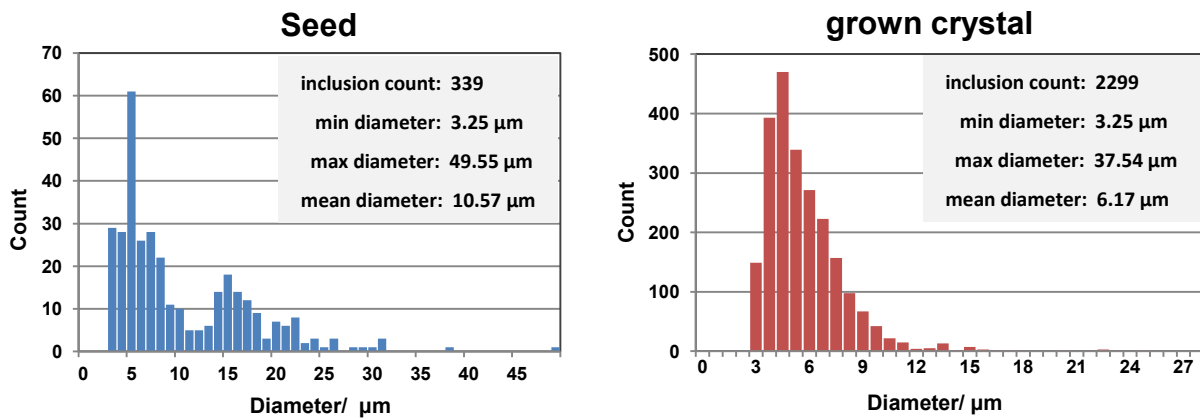


Fig. 3: histogram of the two areas with the same size in sample F1-03-GM. The grown crystal has much more inclusions but with smaller mean diameter (10.57 μm) when compared to the seed (6.17 μm).

In-situ detection of crystallization processes and seed selection in high temperature solutions

Andreas Schneider¹ and Anton Jesche¹

¹*University of Augsburg, Universitätsstraße 2, 86135 Augsburg, Germany*

andreas-gabriel.schneider@physik.uni-augsburg.de

anton.jesche@physik.uni-augsburg.de

Summary

Solution growth is a powerful tool for single crystal growth of various materials [1] and particularly useful for basic research in solid state physics and chemistry. Compared to procedures like Czochralsky or Bridgeman growth it doesn't depend on congruent melting of the respective compound. In contrary, a decrease of the formation temperatures of the desired compounds by several hundred degrees as well as reduced vapor pressures and higher diffusion rates can be achieved. Accessing the exact onset and temperature of nucleation on the other hand remains almost impossible. A prediction of this instant gets also hampered by the uncertainties of the published liquidus temperatures (if available at all). This gets aggravated by supercooling, which stays undetected during the growth procedure. The difference between the displayed furnace temperature and the actual sample temperature makes this even more difficult.

Here we present a way to accurately measure the complete time-temperature profile including small temperature changes caused by dissolution or nucleation. This is achieved by contacting the growth crucible (ceramic) with a measurement wire of high thermal and mechanical stability such as pure or alloyed tungsten. By sawing grooves into the crucible's bottom side and placing the wire into them in a meandering way, the wire gets as close as possible to the melt without direct contact covering a major part of the crucible bottom. An alumina based high temperature ceramic glue with high thermal conductivity covers and stabilizes the wire inside the grooves. By connecting the thin wire with massive metallic rods (3 mm in diameter) of tungsten or molybdenum that lead from the heating zone to the outside of the furnace the voltage at the measurement wire can be detected directly by using a Lock-in amplifier. Due to the linear temperature dependence of the wire resistance, the measured Lock-In voltage directly follows the crucible temperature. Additional contributions by released or absorbed heat inside the solution cause anomalies within this curve. Information about the absolute temperature is provided by a thermocouple the crucible is placed onto during growth.

Without the necessity of a reference crucible, the signal-to-noise ratio approaches the level of conventional DTA-signals. The detection of nucleation enables seed selection using oscillations within a well-defined temperature range. The system can be applied to various solvents including aqueous solutions and has been proven up to 1300°C. Furthermore, promising tests on metallic crucibles such as tantalum have been successfully conducted. The entire measurement setup is placed in a tube furnace, providing high heating and cooling rates, a temperature accuracy of 0.5 Kelvin and stable atmosphere conditions. The reaction chamber can be flooded with inert gas allowing the growth of air sensitive samples as well as protecting metallic crucibles and the measurement wire. The processes are

controlled by a graphical user interface offering the possibility of real time observation of the sample state together with in-situ analysis tools.

Eight well explored binary systems showing phase transitions between 147°C and 1121°C have been investigated and compared with DTA measurements of the same composition. Obtained results are in good agreement with the literature as well with DTA. Single crystals of binary PdBi were investigated in detail and the growth optimized. The obtained crystals were successfully enhanced in size in comparison to conventionally grown ones.

Furthermore they are not only significantly larger but also of excellent quality as shown by the emergence of dHvA-oscillations at comparatively high temperatures and low fields of 3 Tesla at 2 Kelvin. Besides the liquid-solid phase transitions also a solid-solid phase transition of β -PdBi₂ to α -PdBi₂ [2] and vice versa has been detected successfully, showing the sensitivity and versatility of the system.

The established setup offers a considerable increase in efficiency and accuracy for various solution growth processes, suitable for a wide variety of systems. The application to other such growth systems as well as further improvements of sensitivity and precision are anticipated.

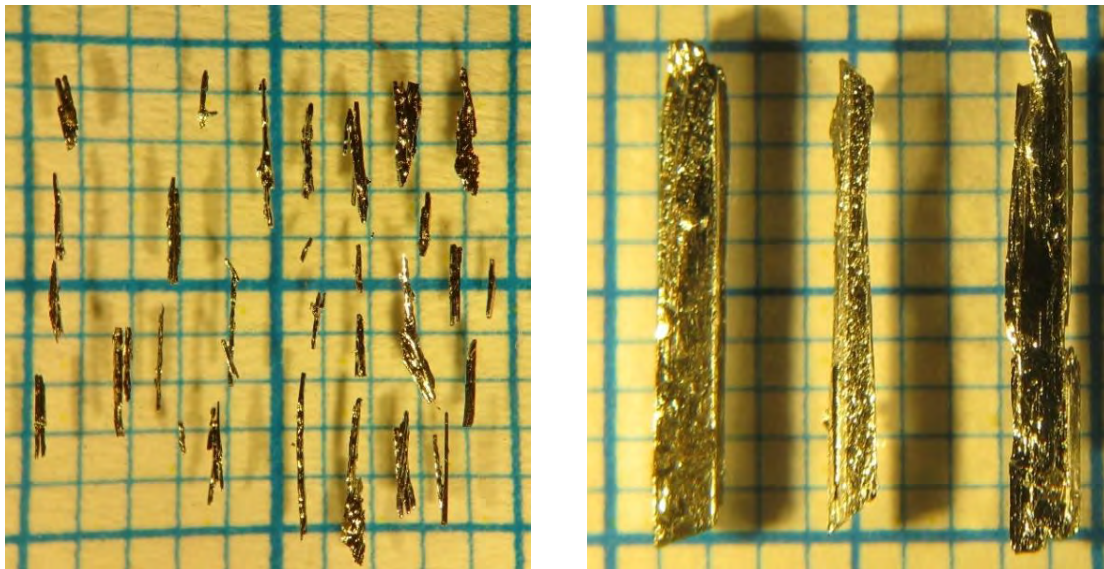


Fig: Conventional grown PdBi-crystals from a box furnace (left) in direct comparison with seed selected PdBi-crystals (right)

Acknowledgment

This work was supported by the Deutsche Forschungsgemeinschaft (DFG, German Research Foundation) - Grant No. JE748/1. The crystal growth apparatus is developed in a cooperative project with the SciDre GmbH, Dresden, with financial support from the ZIM program of the German Ministry for Economic Affairs and Energy (BMWi).

[1] M. M. Kanatzidis, R. Pöttgen, W. Jeitschko, *Angew. Chem. Int. Ed.* **2005**, *44*, 6996.

[2] T. B. Massalski (ed.), *Binary Alloy Phase Diagrams* (Vol. 1), ASM International, Materials Park, OH **1986** → Bi-Pd (Bismuth-Palladium)

[3] A. G. Schneider, P. Sass, R. Schöndube, A. Jesche, *Cryst. Res. Technol.* **2019**, 1900109

A KMC model for homoepitaxial growth of Ga₂O₃

W. Miller^a, Dennis Meiling^b, Robert Schewski^a, Andreas Popp^a, Saud Bin Anooz^a,
and Martin Albrecht^a

^a Leibniz-Institut für Kristallzüchtung (IKZ), Max-Born-Str. 2, 12489 Berlin, Germany

^b Electrical Energy Storage Technology (EET) TU Berlin, Einsteinufer 11, EMH 2, 10587 Berlin, Germany
E-mail: wolfram.miller@ikz-berlin.de

Introduction

β -Ga₂O₃ has recently become of great interest because it is an excellent candidate for power electronics and optoelectronic applications [1,2]. Large progress has been made in the homoepitaxy by MBE, MOVPE, and HVPE. Nevertheless, many details of the process are not yet known. Kinetic Monte Carlo methods are one possibility to gain a deeper inside into the surface kinetics. A set of experiments followed by surface analysis using STEM and AFM give us the possibility to compare both experimental and numerical results. We consider only MOVPE on (100) planes because this was the only surface where step growth was achieved [3–5].

Kinetic Monte Carlo Method

We set up a KMC model, which reflects the structure of Ga₂O₃ with its 8 Ga atoms and 20 O atoms in the unit cell. Ga and O₂ can adsorb. The sticking coefficient is set according to the particular atomic configuration of the surface atoms (details see [6]). Ga and O atoms can diffuse, also GaO_x species can diffuse in *c*-direction. There is evidence from experiments that Ga₂O can desorb [7] and thus, we consider this in KMC. We make a list of all possible events with their probabilities and chose in every iteration one event randomly with respect to its relative probability to the sum of probabilities of all events. The diffusion energies were set in the range of 1.5 eV because a 1D mean field approach for island growth gave a value of this order by comparison with experimental results [4].

Results

We performed runs on flat (on-oriented) and vicinal (6° miscut) surfaces. STEM HAADF images of the surfaces reveal that the terraces are always B1 or B2-plane (see Fig. 1) [8].

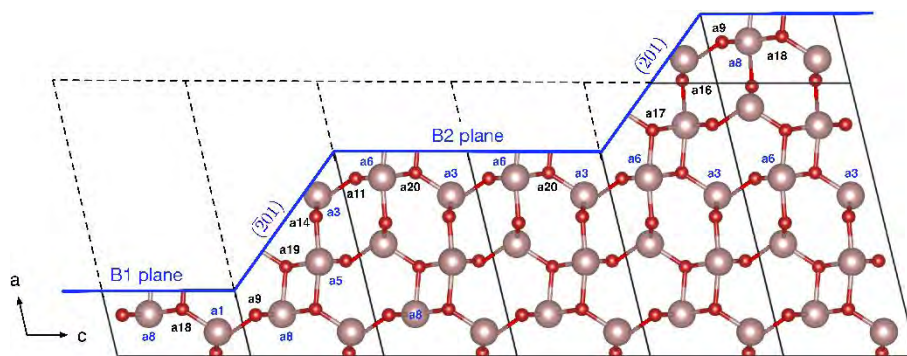


Fig. 1: Surface planes as observed in the STEM analysis. Atoms are labeled according to their number in the KMC code.

On flat surfaces we modify the ratio O/Ga. For small O/Ga ratio no critical nucleus could be formed. The larger the ratio the fast the growth. Nevertheless, no 3D growth is observed but first the next B-plane is filled up. This corresponds with the experimental observations. Choosing a fixed O/Ga ratio we performed

runs for 750°C, 800°C, and 850°C. For the latter we observe large 2D islands as in the experiments [6]. At lower temperature the growth is faster but structure sizes are smaller. On the vicinal surface we change the desorption rates. For an intermediate desorption rate (as used for the flat surface) we obtain step growth (case B in Fig. 2). For high desorption rate (case C) we observe step bunching because every fluctuation in edge growth leads to a growth instability. In the opposite case (case A) we observe random growth on the terraces but eventually ending up in a double step. The final morphology looks similar to that of Case C. Please note that we have only two steps in our KMC run and cannot make any realistic statement beyond the 20 s shown in Fig. 2.

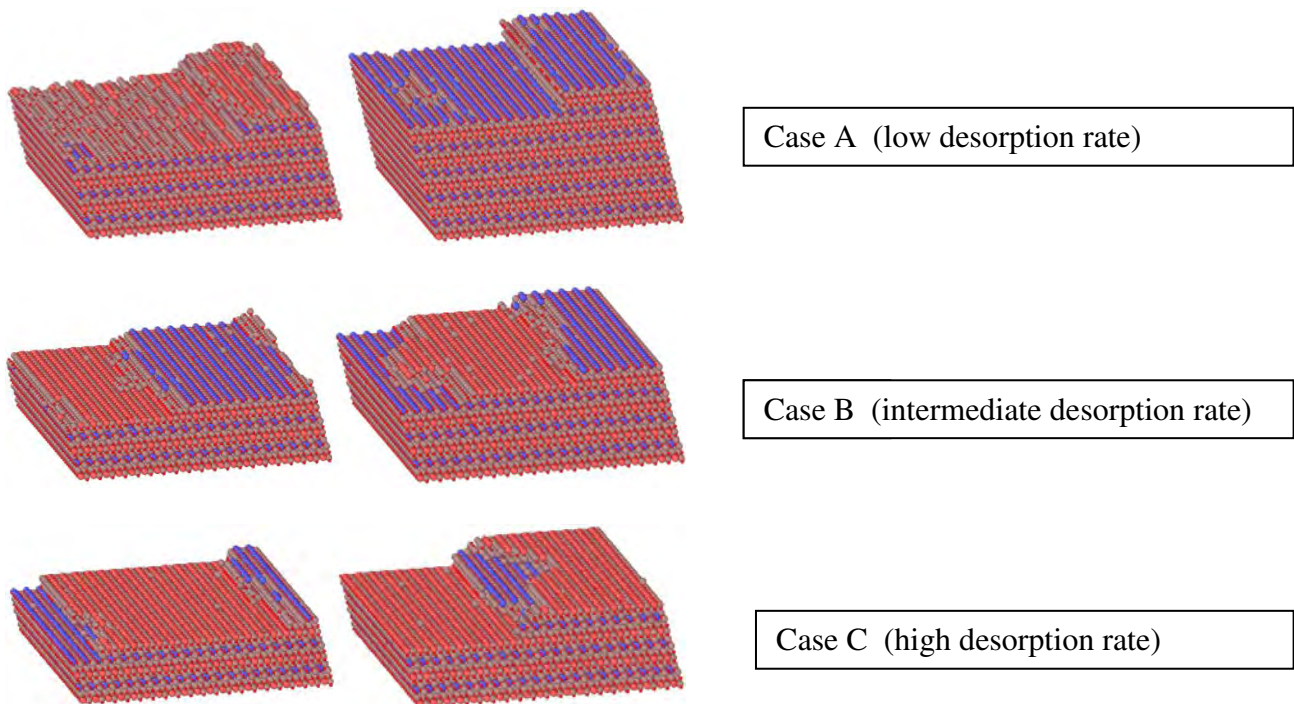


Fig. 2: Surface morphologies for runs with different desorption rates. Left: 10s, Right: 20s.

Acknowledgment

This work was partially conducted in the frame of Science Campus for Growth and Fundamentals of Oxides (GraFox) supported by the Leibniz Association.

- [1] M. Higashiwaki, H. Murakami, Y. Kumagai, A. Kuramata, *Jap. J. Appl. Phys.*, **55**, 1202A1 (2016).
- [2] M. Zhong, Z. Wei, X. Meng, F. Wu, J. Li, *J. Alloys Comp.*, **619**, 572 (2015).
- [3] T. Oshima, N. Arai, N. Suzuki, S. Ohira, S. Fujita, *Thin Solid Films*, **516**, 5768 (2008).
- [4] R. Schewski, M. Baldini, K. Irmischer, A. Fiedler, T. Markurt, B. Neuschulz, T. Remmele, T. Schulz, G. Wagner, Z. Galazka, et al., *J. Appl. Phys.*, **210**, 225308 (2016).
- [5] M.-Y. Tsai, O. Bierwagen, M. E. White, J. S. Speck, *J. Vac. Sci. Technol. A* **28**, 354 (2010).
- [6] W. Miller, D. Meiling, R. Schewski, A. Popp, S. Bin Anooz, M. Albrecht; submitted to *Phys. Rev. Research*
- [7] P. Voigt, O. Bierwagen; *Appl. Phys. Lett.* **109**, 062103 (2016)
- [8] R. Schewski, K. Lion, A. Fiedler, C. Wouters, A. Popp, S. V. Levchenko, T. Schulz, M. Schmidbauer, S. Bin Anooz, R. Grüneberg, et al., *APL Mater.*, **7**, 022515 (2019).

Investigation of soluto-capillary convection in $\text{Ge}_x\text{Si}_{1-x}$ melts

J. P. Wöhrle, T. Jauß, T. Sorgenfrei

Crystallography, Albert-Ludwigs-University Freiburg, Hermann-Herder-Straße 5, 79104 Freiburg,
Germany

E-mail: jan.philipp.woehrle@krist.uni-freiburg.de

The requirements for industrial semiconductor materials used for device applications are constantly rising – one example is the upcoming development of the 5G mobile network technology and the following advancement of autonomous driving. Therefore, high quality bulk crystals are needed – to solve the technical obstacles, a profound comprehension of the respective material systems is required. Especially in mixed systems, additional challenges concerning the homogeneity of the grown material are rising due to varying properties of the different chemical composition of the components, such as germanium and silicon.

$\text{Ge}_x\text{Si}_{1-x}$ is an elemental semiconductor material which is extremely attractive for various applications like thermoelectrics, microelectronics, photovoltaic, or various functional applications due to its lattice constant and band gap tuning based on the composition. A major challenge in growing high quality $\text{Ge}_x\text{Si}_{1-x}$ bulk crystals from melt, is the fact that the surface tension of silicon is 30% higher than germanium, while on the other hand the density is only half as large (see table 1).

Table 1: Surface tension and density of Ge and Si.

	germanium	silicon
surface tension	$\gamma(T) = 591 - 0.08 \cdot (T - T_m)$ mN/m [1]	$\gamma(T) = 765 - 0.016 \cdot (T - T_m)$ mN/m [2]
density	5.323 g/cm ³ at 20 °C [3]	2.336 g/cm ³ at 20 °C [3]

Due to the large segregation coefficient of Si in Ge of $k_0 \leq 5$, germanium is enriched in front of the solid/liquid interface, which leads to a strong soluto-capillary convection and solutal buoyancy convection. It is shown that this specific type of convection is significantly influencing the shape of the solid-liquid interface and consequently the complete growth process, if a growth technique with free melt surfaces is used (e.g. Float-Zone, detached Bridgman, etc.). Therefore, a deeper understanding of the influence of convection flux and capillary phenomena on the resulting crystal quality is needed. Under normal gravity conditions on earth (1g), it is not possible to investigate the effect of the buoyancy force and different surface-tension-driven convections separately on the crystal growth process – in microgravity (μg) the influence of density-driven convection is suppressed including the strong buoyancy convection. These experiments under μg conditions provide the possibility to investigate the flow behavior in-situ on and in the liquid phase without the disturbing impact of the buoyancy convection.

Therefore, we perform experiments in parabolic flights (see fig. 1) which provide several μg phases up to 22 seconds, where we can quantitatively and qualitatively determine the effect of soluto-capillary convection in the Ge-Si system. In the used setup, the solid/liquid interface is running perpendicular to the melt surface so that impacts of surface tension driven flows and their effects on the growth front can directly be observed. By analyzing the movement of small boron nitrite tracer particles on the melt surface during solidification we can track the movement processes and estimate the velocities of these particles. Different $\text{Ge}_x\text{Si}_{1-x}$ mixtures (3-35 at% Si) are used to investigate the effect of the composition on the soluto-capillary Marangoni convection.

To handle the short parabolic phases, we have to ensure that we can heat up and cool down the samples rapidly – therefore we use a double ellipsoid mirror furnace with an argon atmosphere as inert gas (scheme of used furnace in fig. 2). To record the tracer paths (e.g. fig. 3), we use a top mounted high-speed CCD camera. A current view on the results of the parabolic flight campaigns of the last years will be presented.

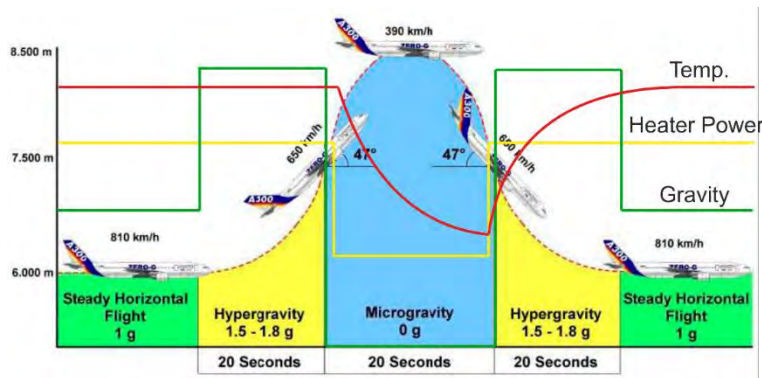


Figure 1: Parabolic flight setup during one parabola (image by Novespace, France). One flight day offers 30 parabolas with 20 seconds of microgravity each. Guaranteed maximum deviations of $\pm 0.005g$.

Figure 2: Left: Double ellipsoid mirror furnace allows rapid heating and cooling of the samples. Right: A high-speed camera above the top window records tracer movements on the solidifying melt surface. The crucible consists of SiC coated graphite.

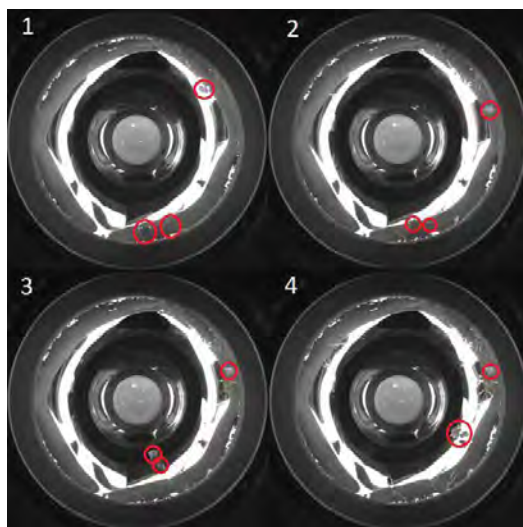
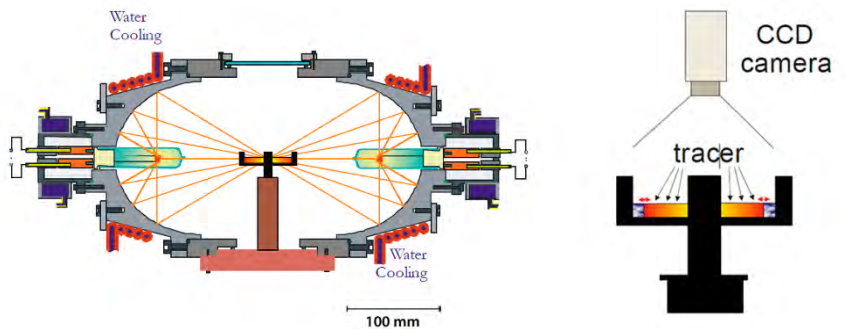


Figure 3: Four stages during a μg experiment: (1) In the initial state, the sample is completely molten. The pBN tracers remain on the starting position. (2) Solidification starts on the top. The tracer is moved by soluto capillary convection and thermocapillary convection. (3) Solidification starts also on the lower crucible wall. Second tracer movement is initiated. (4) In the final state, the complete sample is solid and will be heated again for the next parabola.

[1] Kaiser, N., Cröll, A., Szofran, F.R., Cobb, S.D., Benz, K.W. Journal of Crystal Growth 231 (2001), 4, 448-457

[2] Rhim, W.-K., Ohsaka, K.: Journal of Crystal Growth 208 (2000) 313-321

[3] Greenwood, N.N., Earnshaw, A.: *Chemie der Elemente*. 1. Auflage. VCH, Weinheim 1988, S. 482

Parameter study on n-type multicrystalline ingots with tailored resistivity profiles

I. Buchovska, N. Dropka, M. Pietsch, F.M. Kiessling

Leibniz-Institut für Kristallzüchtung, Max-Born-Str. 2, D-12489 Berlin, Germany

Nowadays multicrystalline silicon (mc-Si) produced by directional solidification (DS) is the most popular substrate material for manufacturing of solar cells. It covers more than 60% of PV market and is expected to keep a significant share in the next decade. The trend towards high efficiency and low cost solar devices results in multiple changes and improvements both in solar cell technology and crystallization methods. One of the most promising concepts is solar cells and modules based on n-type crystalline silicon material, which already demonstrates world record efficiencies and is the most suitable candidate to be the next industry standard. In general, crystallization of standard n-type material does not imply any dramatic changes in comparison to p-type growth. However, some specific differences related to the peculiarities of dopant element still exist. For instance, strong segregation of phosphorus in silicon leads to broader resistivity variation of n-type phosphorus-doped ingots in comparison to p-type ones, which in turn results in lower yield and higher cost of crystalline material.

Recently the method for reduction of resistivity variation in phosphorus-doped directionally solidified mc-Si was proposed. It is based on the ability of phosphorus to evaporate from silicon melt surface not only in case of high vacuum but also at pressures typical for DS crystallisation [1]. The method implies controlling and altering phosphorus transport both in liquid and gaseous phases by the complex arrangements of ambient pressure, gas flow and melt mixing performed by travelling magnetic fields (TMF). It was shown that this approach can be effectively used to control and tailor resistivity distribution along the ingots height. However, it has not yet been investigated how the manipulations with gas pressure and melt mixing affect other parameters of multicrystalline ingots, which are important for solar cell operation.

In this work we present the results for n-type DS-Si ingots, which were grown using complex arrangements on influencing phosphorus transport during growth process. These involve variation of melt stirring, ambient gas flow and gas pressure. In the row of experiments on homogenization of resistivity profiles different process conditions and their combinations were tested on G1-size (22 x 22 x 12 cm³) n-type DS ingots, including both conventional and high performance mc-Si material. The quality of ingots was characterized in terms of minority carrier lifetime, as well as the presence of impurities and inclusions (Cs, Oi, SiC, Si₃N₄, metals etc.)

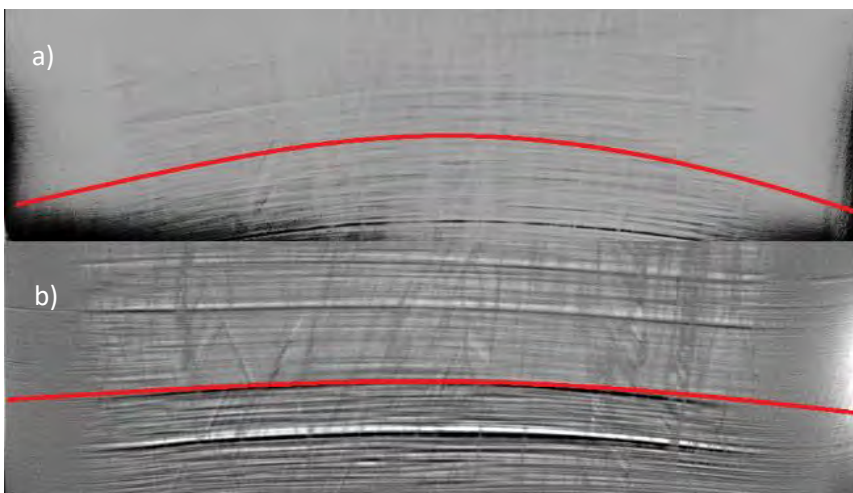


Fig. 1: The shape of solid-liquid interface of mc-Si ingots:
a) without TMF stirring,
b) with TMF stirring

The influence of each process parameter on material quality will be discussed. It will be shown that enhanced melt stirring with double-frequency TMF not only promote uniform resistivity profile in the first half of mc-Si, but also ensures flatter crystallization front (Fig. 1.), which is beneficial for stable crystal growth [2].

A particular attention will be given to the influence of gas pressure on ingot quality and process safety. It is well known that low ambient pressure during crystallization provokes erosion of crucible coating as well as migration of oxygen from a crucible into silicon melt and its evaporation from melt surface [3]. It will be shown that even at the process pressure of 50 mbar no sticking between a quartz crucible and the ingot was observed and no harmful Si_3N_4 inclusions were found in crystallized ingots. The used crucibles were coated with Si_3N_4 according to a developed in-house procedure. Furthermore, although such low pressures result in somewhat increased concentration of O_i in the second half of mc-Si ingots, it was on an acceptable level and significantly lower than regular elevated values at the bottom of DS ingots (Fig. 2).

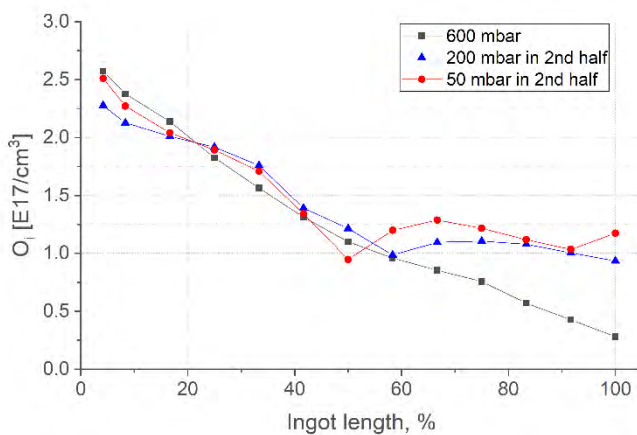


Fig. 2: Distribution of interstitial oxygen for mc-Si ingots grown with different ambient pressure

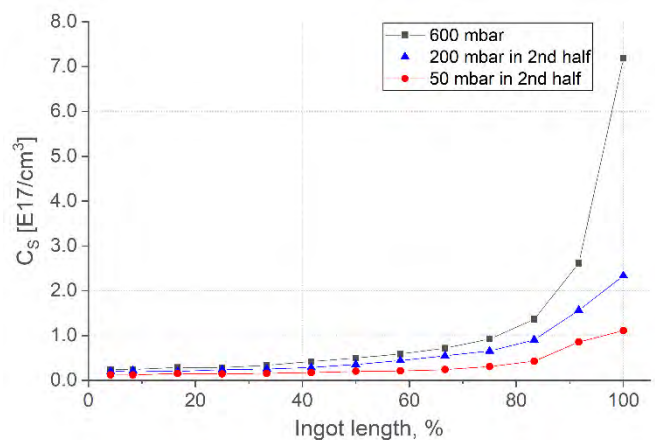


Fig. 3: Distribution of substitutional carbon for mc-Si ingots grown with different ambient pressure

It will be shown that a complex approach to melt stirring and gas transport ensure not only improved resistivity distribution along the height of n-type phosphorus-doped DS-Si ingots, but also provide multicrystalline material of high quality suitable for production of high efficiency solar cells and modules.

Acknowledgment

The authors are thankful to M. Imming-Friedland and T. Wurche for sample preparation.

- [1] I. Buchovska, N. Dropka, S. Kayser, F.M. Kiessling, J. Cryst. Growth, **507**, 299 (2019)
- [2] F.M. Kiessling, F. Büllesfeld, N. Dropka, Ch. Frank-Rotsch, M. Müller, P. Rudolf, J. Cryst. Growth, **360**, 81 (2012)
- [3] X.M. Huang, K. Saitou, S. Sakai, K. Terishima, K.Hoshikawa, Jpn. J. Appl. Phys. **37**, 3188 (1998)

Investigation of directionally solidified quasi-mono silicon for future gravitational-wave detector test-mass mirrors

Frank M. Kiessling^{1,*}, Iryna Buchovska¹, Graeme McGhee², Maya Kinley-Hanlon², Iain Martin², Peter Murray², Roman Schnabel³, Jessica Steinlechner^{4,5}, Simon Tait²

¹Leibniz-Institut für Kristallzüchtung, Max-Born-Str. 2, D-12489 Berlin, Germany

²SUPA, School of Physics and Astronomy, University of Glasgow, Glasgow, G12 8QQ, Scotland

³Institut für Laserphysik und Zentrum für Optische Quantentechnologien, Universität Hamburg, Luruper Chaussee 149, D-22761 Hamburg, Germany

⁴Maastricht University, P.O. Box 616, 6200 MD Maastricht, The Netherlands

⁵Nikhef, Science Park 105, 1098 XG Amsterdam, The Netherlands

*email: frank.kiessling@ikz-berlin.de

In 1916, Albert Einstein predicted the existence of gravitational waves (GW). A century later on 09-14-2015, the Laser Interferometer Gravitational-wave Observatory (LIGO) observed GW from the merging of two black holes for the first time [1]. In order to detect more gravitational waves from a wider range of sources, the detection sensitivity has to be continuously improved. The European Einstein Telescope (ET) is a vision for the next (3rd) generation of GW detectors [2]. One component of the conceptual ET design study are 200 kg test-mass mirrors from single crystalline silicon.

Although there exist various techniques to produce silicon single crystals, the diameter of the crystals is the first criterion to consider. Since the size of a mirror has to be about 50 cm in diameter, single crystalline silicon of highest perfection cannot be provided by the crucible-free float zone technique. Even dislocation free silicon single crystals, which have been grown by the Czochralski (Cz) method, might not fulfill the proposed size and purity required for the Einstein Telescope [2, 3]. An interesting approach to overcome the size problem is the use of silicon grown by directional solidification (DS). DS-Si can be grown as quasi-mono ingots with far bigger sizes needed here and might be available on the market by request. Unfortunately, this quasi-mono silicon has the lowest material quality compared to the dislocation-free silicon crystals mentioned above. But, since the oxygen level in directional solidified silicon material is lower than the one in Cz-Si and even magnetic Cz-Si crystals, the use of DS-Si might be a promising approach. Thus, the defect limits have to be investigated in order to evaluate its suitability for the use as a future gravitational-wave detector test-mass mirrors material.

Samples of different sizes have been prepared using a quasi-mono silicon ingot grown by directional solidification. The material has been characterized regarding carrier lifetime, concentration of substitutional carbon C_s, interstitial oxygen O_i and electrical resistivity. Microwave detected photoconductivity method, FTIR and conductivity measurements are performed, respectively. Additionally, photoluminescence measurements reveal possible recombination active dislocation clusters. These data will be discussed in relation to preliminary results of mechanical loss (which determines the level of thermal noise) and optical absorption (a crucial parameter for maintaining cryogenic operating temperature) values.

References

- [1] B. P. Abbott et al., *Phys. Rev. Lett.* 116, 061102 (2016).
- [2] <http://www.et-gw.eu/index.php/etdsdocument>
- [3] J. Steinlechner, *Phil. Trans. R. Soc. A* 376, 20170282 (2018).

Single crystal growth of Sn- and Ge-substituted GaPd₂ for basic research in catalysis

S. Püschel, K. Bader, and P. Gille

Ludwig-Maximilians-Universität München, Department of Earth and Environmental Sciences,
Crystallography section, 80333 München, Germany
E-mail: stefan.pueschel@campus.lmu.de

Summary

According to recent studies, intermetallic compounds may have better catalytic properties than presently used industrial catalysts that are based on noble metal elements or substitutional alloys from them [1]. The latter ones suffer diffusion and segregation under operation conditions, while intermetallics have well-defined structures with the catalytically active atoms at specific atomic sites. Therefore, they may have better long-term stability and considerably higher catalytic selectivity, according to the *active-site isolation concept* [2].

Several binary compounds in the Ga-Pd system have already been grown with the Czochralski technique from Ga-rich solutions as cm³-sized single crystals [3], which are required for fundamental studies in surface physics and crystallography. The intermetallic compound GaPd₂ has been shown to be the best candidate for heterogeneous catalysis in hydrogenation processes, with catalytically active Pd sites, being well isolated. More recently, it has been found that partially replacing Ga by Sn in GaPd₂ may further increase the activity of this catalyst [4].

Substituting a part of the Ga atoms by an element from the fourth group in the periodic table, thus growing solid solutions, e.g. (Ga,Ge)Pd₂ or (Ga,Sn)Pd₂, allows to study the electronic influence of an additional valence electron on the material's catalytic properties while the crystal structure remains almost unchanged. Unfortunately, little is known about the ternary Ga-Ge-Pd and Ga-Sn-Pd phase diagrams. In the pseudobinary GaPd₂-GePd₂ system, the substitution of Ga by Ge is restricted since GaPd₂ crystallizes in the Co₂Si structure type (*Pnma*) and GePd₂ in the Fe₂P structure type with hexagonal symmetry (*P $\bar{6}$ 2m*). An isothermal section through the ternary phase diagram at 700°C has been published as early as 1975 [6] indicating a maximum Ge substitution according to approx. Ga_{0.57}Ge_{0.43}Pd₂. GaPd₂ and SnPd₂ are isostructural in the Co₂Si structure type (*Pnma*) and therefore form a complete solid solution series. However, pure SnPd₂ cannot be grown from a liquid phase, but decomposes in a peritectoid reaction at 820°C [5]. Thus, ternary Ga_{1-x}Sn_xPd₂ solidification from a native melt or solution is expected to result in an upper limit of Sn substitution for Ga.



Fig. 1: Ga_{0.7}Sn_{0.3}Pd₂ single crystal, grown with the Czochralski technique in [010] direction.



Fig. 2: Ga_{0.8}Ge_{0.2}Pd₂ single crystal, grown with the Czochralski technique in [001] direction.

This contribution presents the results of a high number of slow-cooling experiments in order to investigate parts of the unknown liquidus surface, i.e. to study the primary crystallization fields of the 1:2 phase solid solutions and the relevant tie-lines for the crystal growth in the two ternary systems Ga-Ge-Pd and Ga-Sn-Pd. These small-scale experiments were done with typically less than 1 g of material in graphitized fused silica ampoules. The obtained spherical samples were investigated using X-ray powder diffraction, optical microscopy and electron-probe microanalysis. The maximum Ga substitution by Sn has been determined as $\text{Ga}_{0.46}\text{Sn}_{0.54}\text{Pd}_2$ that primarily crystallized from a solution of composition $(\text{Ga}_{0.4}\text{Sn}_{0.6})_{0.38}\text{Pd}_{0.62}$. Based on these findings, Czochralski growth experiments from incongruent melts, being either (Ga,Sn)- or (Ga,Ge)-rich, were successfully done using binary GaPd_2 seeds of different crystallographic orientations. As already known from growth experiments with binary GaPd_2 , extremely low pulling rates down to $25 \mu\text{m/h}$ were necessary to avoid fluid inclusion formation. Weak segregation effects along the pulling direction (Fig. 3) indicate pseudobinary segregation coefficients that are only slightly lower than unity.

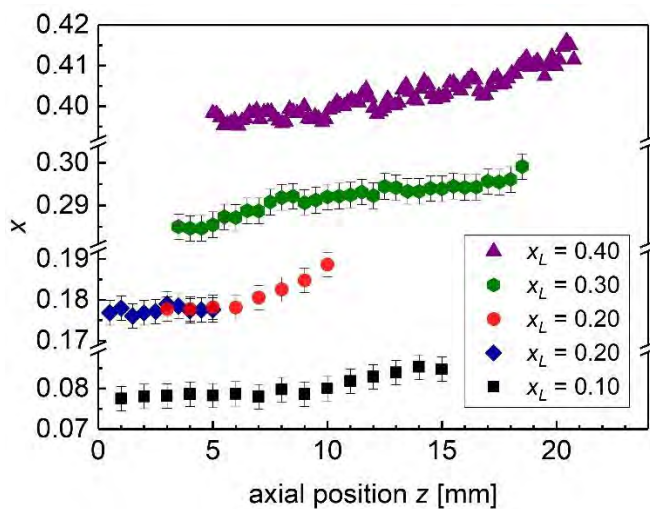


Fig. 3: Axial composition profiles of single crystals of the $\text{Ga}_{1-x}\text{Sn}_x\text{Pd}_2$ solid solution grown from different starting melts. The Sn content of the starting charge is given in terms of the pseudobinary mole fraction x_L according to $(\text{Ga}_{1-x_L}\text{Sn}_{x_L})_{1-y_L}\text{Pd}_{y_L}$ [7].

Acknowledgments: The authors are grateful to Juri Grin (MPI for Chemical Physics of Solids, Dresden) and Marc Armbrüster (TU Chemnitz) for fruitful discussions as well as to the Deutsche Forschungsgemeinschaft for financial support under grant no. GI 211/15-1.

References

- [1] M. Armbrüster, R. Schlögl, Yu. Grin, *Sci. Technol. Adv. Mater.*, **15**, 1-17 (2014).
- [2] W.M.H. Sachtler, *Catal. Rev. Sci. Engin.*, **14**, 193-210 (1976).
- [3] J. Schwerin, D. Müller, S. Kiese, P. Gille, *J. Crystal Growth*, **401**, 613-616 (2014).
- [4] O. Matselko, R.R. Zimmermann, A. Ormeci, U. Burkhardt, R. Gladyshevskii, Yu. Grin, M. Armbrüster, *J. Phys. Chem. C* **122**, 21891–21896 (2018).
- [5] T.B. Massalski et al., *Binary Alloy Phase Diagrams*, ASM International, Ohio (1990).
- [6] S. Heinrich, K. Schubert, *Z. Metallkd.* **66**, 353-355 (1975).
- [7] K. Bader, A. Dorner, P. Gille, *J. Crystal Growth*, **532**, 125401 (2020).

Thermally stimulated dislocation generation in silicon crystals grown by the Floating Zone method

Hans - Joachim Rost, Iryna Buchovska, Kaspars Dadzis, Uta Juda, Robert Menzel, Matthias Renner*

Leibniz-Institut für Kristallzüchtung, Max-Born-Str. 2, 12489 Berlin, Germany

**email: hans-joachim.rost@ikz-berlin.de*

Previously, the dislocation behavior from the view point of photovoltaics was studied during melting and crystallization of large-area single crystal seeds at near-equilibrium conditions using the so-called NeoGrowth technique [1], [2]. Alternatively, the authors investigated the crucible-free growth of low-defect single crystals on large-diameter silicon seeds by a new, modified FZ- technique [3] without using the common Dash technique. All grown crystals, independent of the seed structure or preparation procedure, reproducibly developed a dislocation network in the temperature range between 900 °C and 1200 °C already during heating to the melting temperature and before the growth started.

In the present study, a long dislocation-free crystal with a diameter of 20 mm and smaller than the inner hole diameter of the RF-coil was grown using the standard Floating Zone method. Then the grown crystal, without any mechanical or chemical treatment, was stepwise heated up in the temperature range from 700 °C till 1180 °C controlled by a pyrometric system. After reaching a quasi-stationary state for a chosen temperature, the crystal was shifted by a certain distance relative to the fixed coil. The crystal was then cut into segments of about 100 mm in length. Plates with a thickness of 2 mm were cut parallel to the growth direction and double-side polished. Additionally, wafers were cut perpendicular to the growth direction between the segments. The samples were analyzed by Lateral Photovoltage Scanning (LPS), photoluminescence (PL) and etch pit density (EPD) as well as the lifetime were measured.

Comparing the results of the different methods a strong correlation between the dislocation density and the lifetime was found in dependence of the temperature increase in the investigated range. The region of the dislocations generation and its spreading behavior could be revealed. Possible origins and correlations will be discussed.

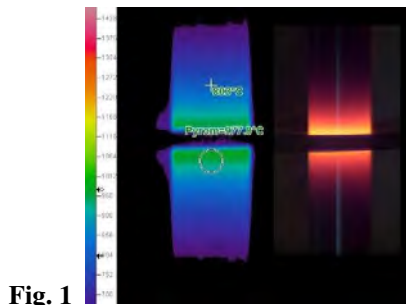


Fig. 1

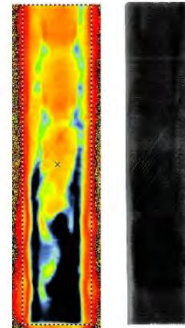


Fig. 2

Figure 1 – Temperature (pyrometer)(left) and crystal picture (right) during the heating.

Figure 2 – Lifetime (left) and EPD (right) measured on a longitudinal cut

References:

- [1] N. Stoddard, B. Gründig-Wendrock, A. Krause, D. Oriwol, M. Bertoni, T. Uberg Naerland, I. Witting, L. Sylla, J. Crystal Growth 452 (2016) 272–275.
- [2] N. Stoddard, J. Russell, E.C. Hixson, H. She, A. Krause, F. Wolny, M. Bertoni, T. Uberg Naerland, L. Sylla, W. von Ammon, Prog. Photovolt. Res. Appl. (2018) 1–8.
- [3] H.-J. Rost, R. Menzel, D. Siche, U. Juda, S. Kayser, F.M. Kießling, L. Sylla, T. Richter Journal of Crystal Growth 500 (2018) 5–10

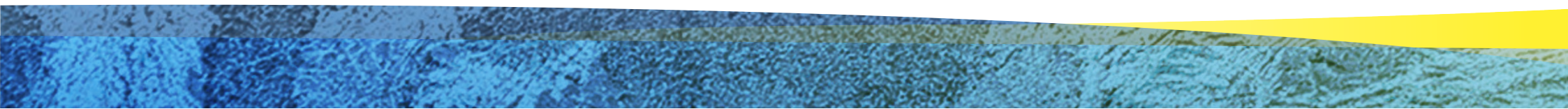


Crystals (ISSN 2073-4352) is an open access journal that covers all aspects of crystalline material research. *Crystals* provides a forum for the advancement of our understanding of the nucleation, growth, processing, and characterization of crystalline and liquid crystalline materials. Their mechanical, chemical, electronic, magnetic, and optical properties, and their diverse applications, are all considered to be of importance. Additionally, we encourage contributors to send articles focused on crystals research (of small and high molecular weight). Their characterization by using modern techniques for crystal growth and high resolution characterization such as synchrotron radiation and modern methods for the growth of crystals for X-ray free electron lasers (XFELS) would also be welcome.

IMPACT
FACTOR
2.06

<https://www.mdpi.com/journal/crystals>

Crystals sponsored the Special Prize of the Scholar's Competition „Wer züchtet den schönsten Kristall“.



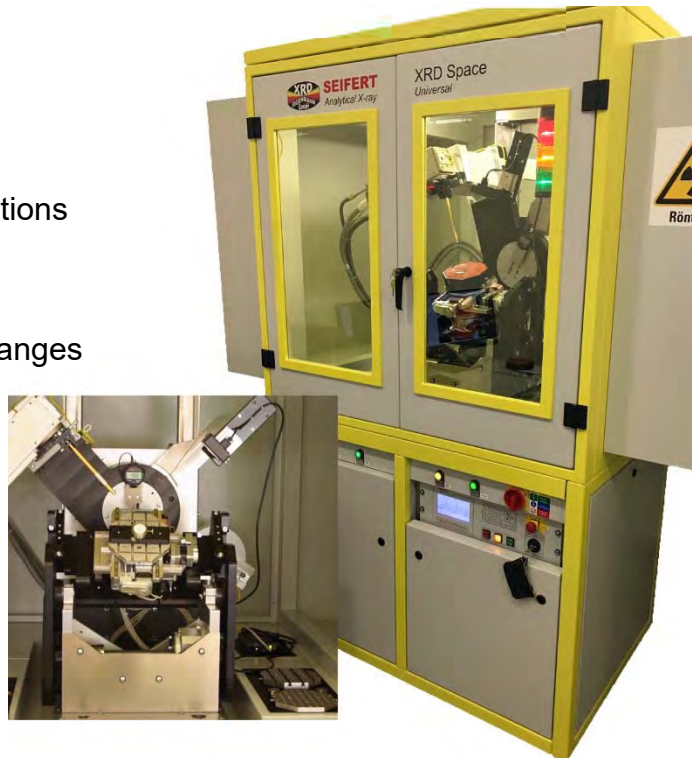
X-ray diffraction systems

... highly precise
... versatile
... customized

XRD diffractometers for
stress analysis
texture analysis
phase analysis
high resolution applications

- XRD Space universal
large sample space
large angular and translation ranges
- XRD Charon SXL
largest sample space
largest sample weight

versatile, camera-controlled sample
mounting
automatic positioning and sampling
of large sample batches



XRD crystal orientation systems

- XRD Galaxy SCL
precision laue systems for fast ori-
entation of crystals, ingots, wafers,
turbine blades
- XRD Galaxy SCD
high precision scanning systems for
orientation of ingots and wafers

versatile, camera-controlled sample
mounting
automatic positioning and sampling of
large sample batches



Ihre Spezialisten für Diamantdrahttechnologie

www.didras.com

Über DIDRAS:

DIDRAS GmbH wurde 2019 aus einem Steinbeis Forschungsinstitut heraus gegründet. Die Technologie des Diamantdrahtsägens verfolgen wir schon seit 2009 durch mehrere Forschungs- und Entwicklungsprojekte.

Technologie:

Das Diamantdrahtsägen überzeugt mit einem präzisen Schnitt und nahezu geschliffenen Oberflächen. Beinahe alle Werkstoffe können durch das Diamantdrahtsägen getrennt werden. Besonders geeignet ist der Diamantdraht zum Trennen von sehr harten und spröden Werkstoffen.

Mit den sehr dünnen Drahtschlaufen von DIDRAS, können kleine Bauteile wie zum Beispiel Elektronik-Widerstände getrennt werden.

Produkt:

- DWLS-650 die CNC-gesteuerte Diamantdrahtsäge
- Für 2D-Schnitte
- Schnittgeschwindigkeit bis zu 80m/s
- Verfahrweg in X/Y = 200 mm
- Drahtschlaufen in allen Längen von 120µm bis 240µm Draht-Ø



HK-Präzisionstechnik GmbH

Kooperationspartner zu DIDRAS GmbH für die Entwicklung und Herstellung von Diamantdrahtsägen für den industriellen Einsatz.

Mehr als 70 Jahre Erfahrung und eine ganz besondere Auffassung von Qualität, Zuverlässigkeit und Präzision begründen heute den herausragenden Ruf der HK-PRT. Besonders auf dem Spezialgebiet der Diamantdrahtsäge-Technik und deren Anwendung in der Siliziumbearbeitung setzt die HK-PRT Technologie neue Maßstäbe.



aprotec – advanced process technologies

Unser Name steht für innovative und fortschrittliche Lösungen in der Prozessanlagen- und Automatisierungstechnik

Prozessanlagentechnik

Entwicklung und Herstellung von schlüsselfertigen Anlagen für kundenspezifischen Prozesse mit speziellen Prozessumgebungen wie Vakuum, Überdruck, hohen Temperaturen oder reinsten Gasatmosphären für die industrielle Produktion oder im Labormaßstab für folgende Anwendungen:

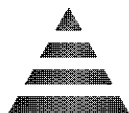
- Kristallzüchtung
- Schmelzen & Gießen
- Tempern, Reduktion und Synthese
- spezielle Hochtemperaturprozesse
- Spezielle Vakuum-/Hochdruckprozesse



Dafür steht unser Team aus Ingenieuren und Technikern mit fundiertem Wissen und langjähriger Branchenerfahrung.

Material-Technologie & Kristalle für Forschung, Entwicklung und Produktion

- ▲ Kristallzüchtungen von Metallen, Legierungen und Oxiden
- ▲ Kristallpräparation (Formgebung, Polieren und Orientieren)
- ▲ Reinstmaterialien (99,9 – 99,99999 %)
- ▲ Substrate (SrTiO_3 , MgO , YSZ , ZnO , Al_2O_3 , etc.)
- ▲ Wafer (Si, Ge, ZnTe, GaAs und andere HL)
- ▲ Sputtertargets
- ▲ Optische Materialien (Fenster, Linsen, etc.)
- ▲ Auftragsforschung für Werkstoffe und Kristalle



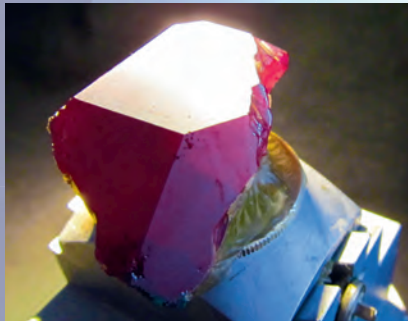
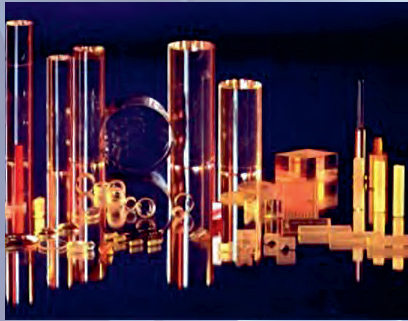
MaTeck

Im Langenbroich 20
52428 Jülich
Tel.: 02461/9352-0
Fax: 02461/9352-11
eMail: info@mateck.de

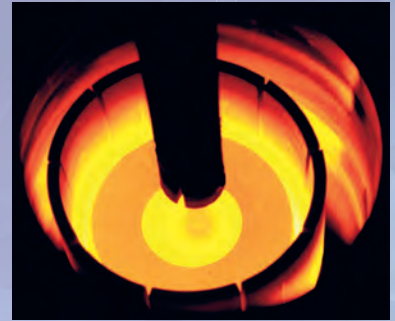
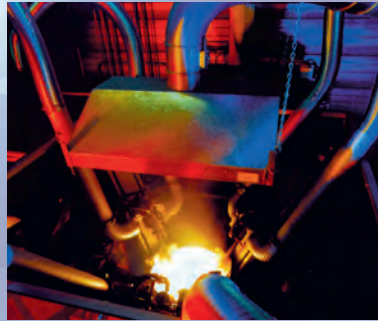
Besuchen Sie uns im Internet (inkl. Online-Katalog):
www.mateck.de

SurfaceNet

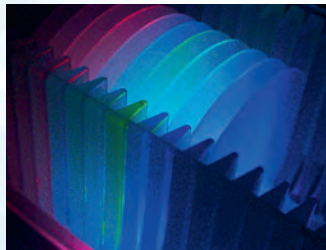
Crystals



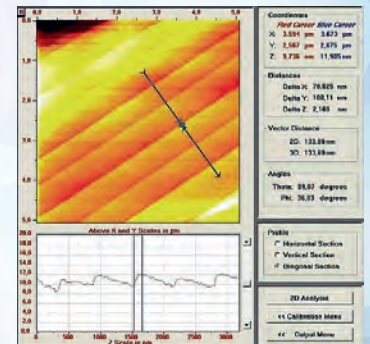
Crystal Puller



Wafers



Analytical Services



Substrates

Custom Parts

Sputter Targets

PLD Targets

Custom Crystal Growth

SurfaceNet GmbH

Oskar-Schindler-Ring 7 · 48432 Rheine – Germany

Fon +49 (0)5971 4010179 · Fax +49 (0)5971 8995632

sales@surfacenet.de · www.surfacenet.de

- Reine und hochreine Metalle & Anorganika
- Aufdampfmaterialien
- Sputtertargets
- Seltene Erden
- Edelmetall-Halbzeuge



chemPUR
Ihr Partner für Chemie & Physik

ChemPur Feinchemikalien und Forschungsbedarf GmbH

Rüppurrer Straße 92
D-76137 Karlsruhe

Tel.: + 49 (0) 7 21 - 9 33 81 40
info@chempur.de **www.chempur.de**



SCIDRE

SCIENTIFIC INSTRUMENTS DRESDEN GMBH

Exploitation of ideas towards novel research equipment



**You have research equipment ideas which are waiting for realization?
You use self-developed technology for your research?**

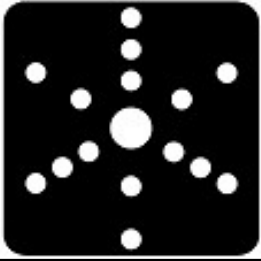


**Contact us to benefit from commercialization of your ideas and for
joint R&D projects towards novel equipment in your lab!**

- Research technologies also have market potential — together we can make successful products out of your equipment ideas!
- Working in science and bringing ideas to the market is compatible — with the right partner there is no impairment of your scientific work
- You earn license fees on every sold product and benefits from successful technology transfer
- You do not bear entrepreneurial risk and become visible as inventor
- We will advise you concerning third-party funds during joint R&D projects

Scientific Instruments Dresden GmbH
Gutzkowstraße 30
01069 Dresden
Germany

Web page www.scidre.de
E-mail info@scidre.de
Phone +49 (0) 351 - 84 22 14 70
Fax +49 (0) 351 - 84 22 89 38



MULTIWIRE LABORATORIES, Ltd.
 95 Brown Rd. MS 1018
 266A Langmuir Building
 Ithaca, NY 14850
Phone: (607) 257-3378
Email: salesinfo@multiwire.com

LAUE-CAMERA GmbH
 Sonnenweg 4b
 85386 Eching
Tel. 0170- 8238306
salesinfo@lauecamera.com
www.lauecamera.com

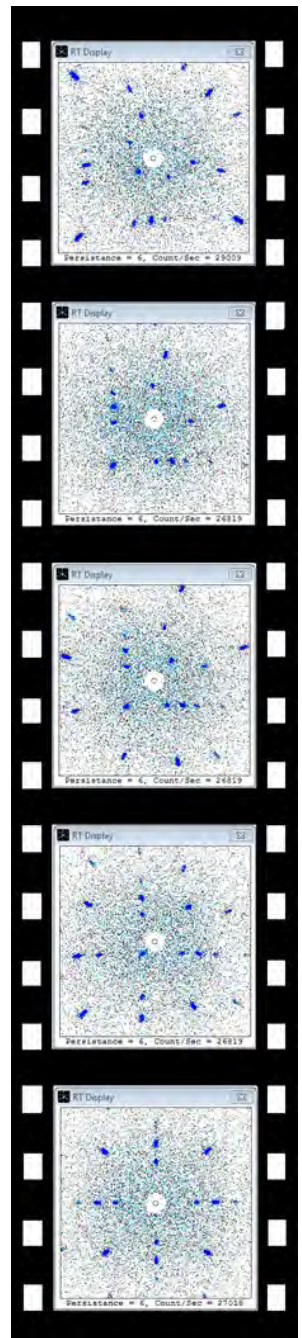
MWL120 Real-Time Back-Reflection X-Ray Camera System



MWL120 REAL-TIME LAUE DETECTOR

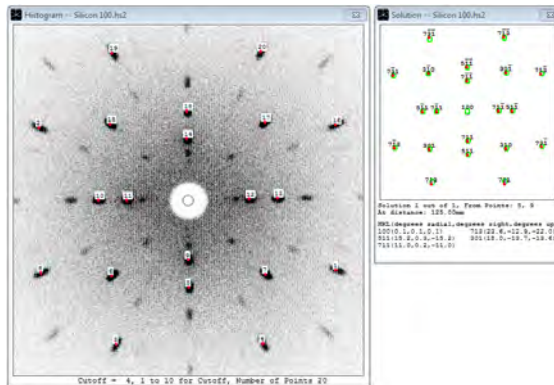
- Ideal replacement for the Polaroid XR-7 back-reflection cassette (film no longer available)
- NorthStar 7 indexes cubic, hexagonal, triclinic crystal systems and creates stereographic projections
- Provides an accuracy of 0.25° in standard Laue mode and 0.05° in high-resolution mode
- Operates best with the MWL motorized orientation stages
- Ideal for research applications, industrial process control, or academic laboratories
- Earlier model MWL110 systems can be upgraded to MWL120 capability

REAL-TIME IMAGE SEQUENCE



NORTHSTAR SOFTWARE

Crystal orientation is fast and easy with the latest NorthStar 7 software. Display real-time images while you rotate your sample, then use the collection mode to capture histograms for analysis. Northstar can automatically detect diffraction spots, determine the Miller index for each reflection, and calculate the angles to any crystal axis, all with a simple point-and-click interface.



Indexed Histogram

MOTORIZED CRYSTAL ORIENTATION

Motorized sample stages allow manipulation of your sample position and orientation during measurements, improving productivity and safety.

- The **MWL706 Three-Axis Motorized Goniometer** makes positioning crystal samples fast and easy with real-time adjustment of pitch, yaw, and roll for samples up to 1 kg in size.
- The **MWL701A Jack & Translation Stage** allows easy vertical and horizontal motion to place the sample correctly in the beam or to image different parts of larger samples.
- The **MWL703 Motorized Bond Barrel** is ideal for orienting crystals



MWL706 3-Axis Goniometer



for **MWL701 Jack & Translation**



MWL703 Motorized Bond Barrel

Abstract Book
DKT2020

ISBN 978-3-00-064845-8

Copyright and responsible :

Deutsche Gesellschaft für
Kristallwachstum und Kristallzüchtung e.V.
DGKK e.V. (WW6, z.Hd. P. Wellmann)
Martensstr. 7
91058 Erlangen
Germany

Editor:
Prof. Dr. Andreas Erb
Walther Meissner Institut
für Tieftemperaturforschung
Bayerische Akademie der Wissenschaften
Walther-Meissnerstr. 8
85748 Garching
Germany



Fraunhofer

IISB

FRAUNHOFER-INSTITUT FÜR INTEGRIERTE SYSTEME UND BAUELEMENTE TECHNOLOGIE IISB

DU BIST STUDENT/-IN
DER ELEKTROTECHNIK,
MECHATRONIK,
WERKSTOFF-
WISSENSCHAFTEN, PHYSIK,
ENERGIETECHNIK ODER
EINES VERGLEICHBAREN
STUDIENGANGS?
STARTE JETZT DEINE
KARRIERE AM
FRAUNHOFER IISB
IN DEN BEREICHEN
LEISTUNGSELEKTRONIK &
HALBLEITERTECHNOLOGIE.



www.recruiting.fraunhofer.de

BEWERBERPORTAL:

www.IISB.fraunhofer.de/jobs